University of Mississippi

eGrove

Honors Theses

Honors College (Sally McDonnell Barksdale Honors College)

Fall 2018

Electro- and Photocatalytic Carbon Dioxide Reduction with Mononuclear and Dinuclear Rhenium Polypyridyl Complexes

Eva Amatya

Follow this and additional works at: https://egrove.olemiss.edu/hon_thesis

 Part of the Chemistry Commons

Recommended Citation

Amatya, Eva, "Electro- and Photocatalytic Carbon Dioxide Reduction with Mononuclear and Dinuclear Rhenium Polypyridyl Complexes" (2018). *Honors Theses*. 1567.
https://egrove.olemiss.edu/hon_thesis/1567

This Undergraduate Thesis is brought to you for free and open access by the Honors College (Sally McDonnell Barksdale Honors College) at eGrove. It has been accepted for inclusion in Honors Theses by an authorized administrator of eGrove. For more information, please contact egrove@olemiss.edu.

Electro- and Photocatalytic Carbon Dioxide Reduction with Mononuclear and Dinuclear Rhenium Polypyridyl Complexes

By

Eva Amatya

A thesis submitted to the faculty of the University of Mississippi in partial fulfillment of the requirements of the Sally McDonnell Barksdale Honors College.

Oxford

December 2018

Approved by

_____

Advisor: Dr. Jonah Jurss

_____

Reader: Dr. Davita Watkins

_____

Reader: Dr. Gregory Tschumper

© 2018

Eva Amatya

ALL RIGHTS RESERVED

Acknowledgements

I would like to thank Dr. Jonah W. Jurss for providing me with the opportunity to work in the lab, trusting me with a very insightful project, guiding and supporting me through every step of my project. I would like to thank all of the researchers in the Jurss Lab, especially Ms. Sayontani Sinha Roy for being an excellent mentor and guiding me through every detail in the lab. I would like to thank my family and friends for their immense support. I would like to thank Shakeiya Davis and the Delcamp Group for their collaboration involving photocatalysis. Above all, I would like to thank the Sally McDonnell Barksdale Honors College for encouraging me and funding this project.

Abstract

The main challenge of reducing carbon dioxide (CO_2) to value-added products lies in designing more efficient catalysts that are long-lived, selective, and operate near the thermodynamic potential for the reaction. In this work, mononuclear and dinuclear Re complexes containing diamine ligands linked to a pendant anthracene moiety have been synthesized and studied for both electrocatalytic and photocatalytic CO_2 reduction. Electrocatalytically, the performances of both catalysts were studied in *N,N*-dimethylformamide (DMF) and acetonitrile (MeCN) solutions to determine their turnover frequencies (TOFs) for C_{O2} reduction. Catalyst performance was compared to previously reported rhenium systems, and both systems studied here were shown to outperform the benchmark catalyst, $Re(bpy)(CO)_3Cl$, in electrochemical and photochemical CO_2 reduction to carbon monoxide (CO).

TABLE OF CONTENTS

Introduction

Carbon dioxide (CO_2) is an integral component of our ecosystem. From being one of the primary reactants of natural photosynthesis by which all living organisms depend for survival to playing a vital role in regulating Earth's surface temperature through the greenhouse gas effect, CO_2 is an important gas in our atmosphere.[1] However, since the Industrial Revolution, the demand for natural resources such as coal, oil, and natural gas as fuels for combustion energy has skyrocketed resulting in a significant increase in the concentration of CO_2 in the atmosphere (**Figure 1**). This elevation of atmospheric CO_2 has led to harmful consequences, namely climate change, ocean acidification, and melting of polar ice caps.[2]

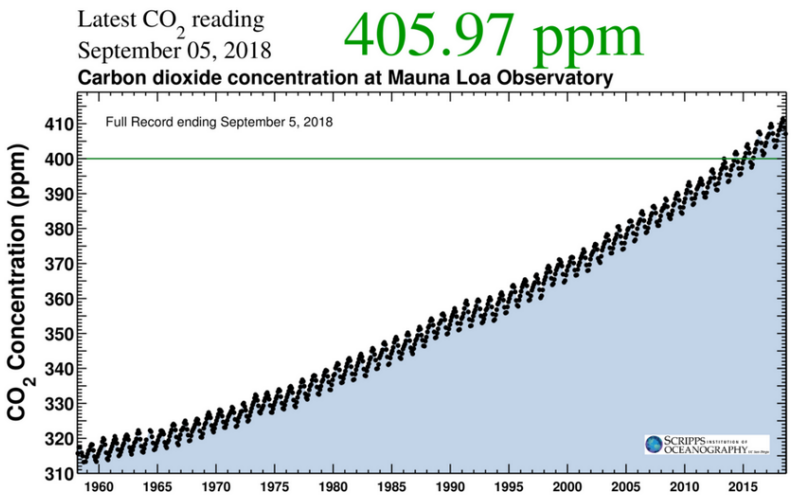

Figure 1. Atmospheric CO_2 concentrations (in ppm) measured at the Mauna Loa Observatory over the last six decades (1958 – 2018).[3]

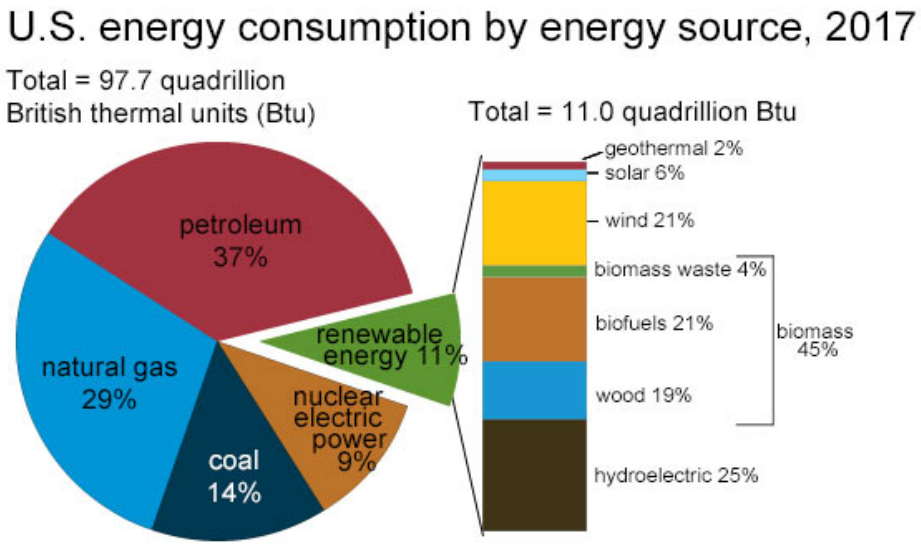

Figure 2. Energy consumption in the United States by energy source for the year 2017.[4]

In 2017 alone, total energy consumption of the United State of America was 97.7 quadrillion Btu among which 89% of the energy consumed was in the form of nonrenewable sources (**Figure 2**). The consumption of fossil fuels (coal, oil, and natural gas) results in CO_2 emissions in the atmosphere as a primary by-product of their combustion. Carbon dioxide is a greenhouse gas, whose ongoing accumulation in the atmosphere has been linked to climate change and other environmental concerns.

By 2050, the Energy Information Agency (EIA) projects a 56% increase in energy consumption.[5] There has been a significant increase in CO_2 levels from 280 ppm to over 400 ppm during the last few decades which is above the desired threshold for atmospheric CO_2 concentration.[3] In this context, one strategy being pursued by the scientific community to alleviate greenhouse gas emissions and find alternative fossil fuel replacements is to generate renewable fuels. The concept of storing energy in the form of chemical bonds and reducing CO_2 back into useful products hails from natural photosynthesis. Using a similar mechanism as found in plants,

catalysts must be designed and developed for CO_2 reduction in order to facilitate the conversion of carbon dioxide into a sustainable chemical fuel. In this manner, the fuel will be burned as usual, but in a closed carbon cycle where the CO_2 by-product following combustion can be reduced back into the fuel, avoiding its accumulation in the atmosphere. Fuels generated by natural or artificial photosynthesis are thus carbon-neutral and do not result in a *net* increase in CO_2 emissions.

Natural and Artificial Photosynthesis

Natural photosynthesis is the process of capturing energy in the form of sunlight to drive the conversion of carbon dioxide and water into complex organic compounds such as glucose which is a building block of living organisms. In this process, water oxidation occurs in Photosystem II to evolve oxygen and provide protons and electrons for the reductive half-reaction that is ultimately CO_2 reduction in the Calvin cycle (**Figure 3**). Notably, the oxygen released in the atmosphere is an environmentally benign, indeed beneficial, by-product of water oxidation.[6] While this work is focused on the development of catalysts for CO_2 reduction, other groups are working on developing better catalysts for the water oxidation reaction as well.

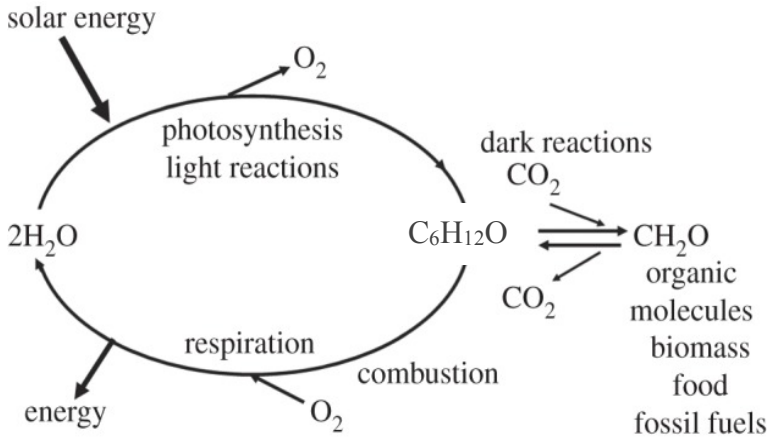

Figure 3. Basic representation of natural photosynthesis.[6]

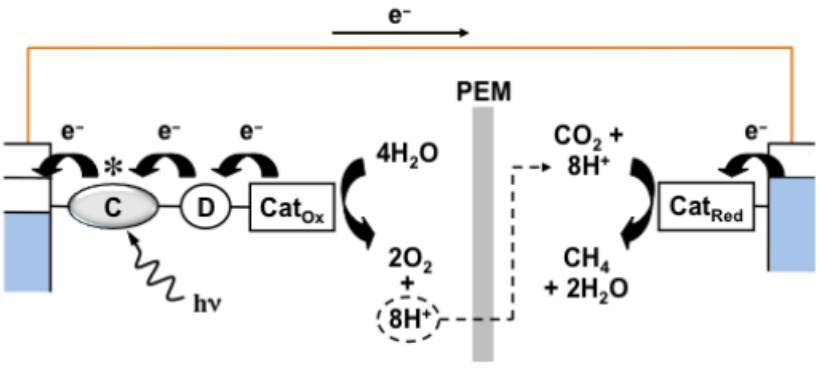

Figure 4. Mechanism of Photoelectrochemical Cell (PEC).[10]

CO_2 Reduction

CO_2 can be reduced to many useful fuels such as methanol, formic acid, carbon monoxide, and ethylene as depicted in **Figure 5**, which can be used as commodity chemicals and fuels. Carbon monoxide, the most common CO_2 reduction product, can be used commercially as a component of syngas (CO and H_2) in the Fischer-Tropsch process to produce long chain hydrocarbons that make up diesel and jet fuels.[13] Although CO is a harmful gaseous product, it frequently serves as a vital raw product used in many industrial processes.

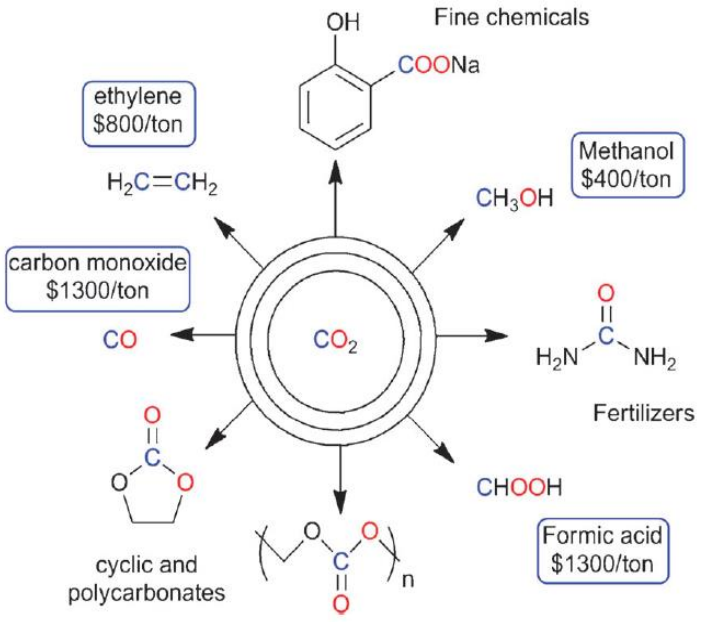

Figure 5. Various products that can be generated from carbon dioxide.[11,12]

Table 1: Thermodynamic potentials for CO_2 reduction to various products at pH 7.[11,14]

Electrochemical reduction of CO_2 in the presence of a proton source (aqueous solution, pH 7, V vs. NHE)	
Selected reduction reactions of CO_2	E^0 / V

$CO_2 + e^- \rightarrow CO_2^{\cdot -}$	-1.90
$CO_2 + 2H^+ + 2e^- \rightarrow CO + H_2O$	-0.53
$CO_2 + 2H^+ + 2e^- \rightarrow HCO_2H$	-0.61
$CO_2 + 6H^+ + 6e^- \rightarrow CH_3OH + H_2O$	-0.38
$CO_2 + 8H^+ + 8e^- \rightarrow CH_4 + 2H_2O$	-0.24

Thermodynamically, it is more efficient to reduce CO_2 at a potential that is close to the thermodynamic potential of the specified reaction (**Table 1**). Conversion of CO_2 to CH_4 is more thermodynamically favorable than conversion of CO_2 to CO since CO_2 reduces at -0.24 V for CH_4 and at -0.53 V for CO at pH 7. However, kinetically, it is easier to transfer 2 electrons and 2 protons in a system rather than 8 electrons and 8 protons, so it is rare that catalysts reduce CO_2 by more than 2 electrons. The one-electron reduction of CO_2 to $CO_2^{\bullet -}$ is an energetically demanding process, because the resulting CO_2 radical anion is a very unstable and reactive intermediate. Thus, multiple electron reduction pathways are available and at substantially lower potentials.[15]

Selectivity is an important factor for a catalyst, because proton reduction is a competing reaction to CO_2 reduction. The thermodynamic potential for proton reduction occurs at -0.42 V at pH 7, making it an easier reaction than carbon dioxide reduction to CO, which occurs at -0.53 V. Since, our objective is to perform carbon dioxide reduction, it is incredibly important for our catalyst to be selective for CO_2 reduction in the presence of a proton source, which is needed as each of the reactions are proton-coupled reductions (**Table 1**). We note that proton-coupled electron transfer (PCET) can avoid the formation of high-energy radical species that would be produced by single electron transfer, which may allow access to lower overpotentials.[12]

Rhenium metal catalysts and Previous works:

Transition metals possess the capability to perform the catalytic reduction of CO_2 due to their ability to adopt multiple redox states and form coordination complexes.[7] A number of different metals have been employed in transition metal complexes, which have been widely investigated for catalytic CO_2 reduction. Rhenium-based catalysts are well-known in the literature due to their durability and superior catalytic activity and selectivity. One of the most common and extensively studied transition metal catalysts is the rhenium (2,2'-bipyridyl)-based system, originally reported by Lehn and co-workers in 1983.[16] Many mononuclear catalysts derivatives based on the benchmark catalyst, $Re(bpy)(CO)_3Cl$, have been developed for electro- and photocatalytic CO_2 reduction over the last four decades. However, significantly less studied are dinuclear systems that may allow for the accumulation of multiple reducing equivalents at lower potentials to facilitate the efficient multielectron reduction of carbon dioxide.

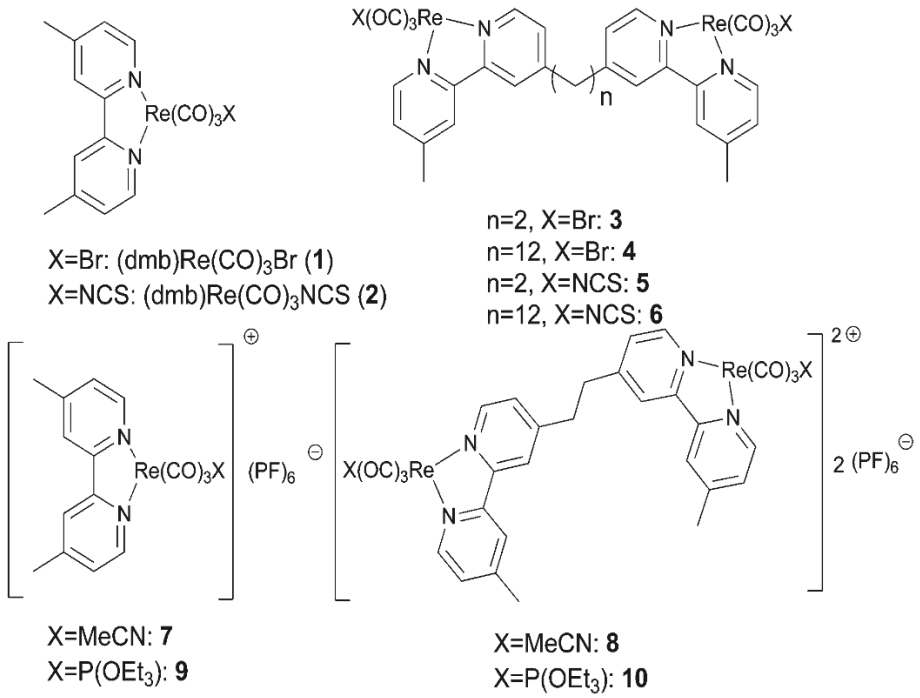

Figure 6. Monomeric and dimeric catalysts developed by the Rieger Group.[17]

Dinuclear rhenium complexes with 1,2-bis(4,4′-methyl-[2,2′]bipyridyl)-ethane and 1,2-bis(4,4′-methyl-[2,2′]bipyridyl)-dodecane as bridging ligands, and (dmb)$Re(CO)_3X$ (dmb is 4,4'-dimethyl-2,2'-bipyridine) were synthesized and their photocatalytic performances were studied and compared by the Rieger Group.[17] They first synthesized a series of mononuclear complexes of the type (dmb)$Re(CO)_3X$, where X = Br^-, NCS^-, MeCN, and $P(OEt_3)$, along with their dinuclear analogues. Through UV-Vis absorption spectra of the mononuclear and dinuclear complexes, they found that alkyl linkers did not have a significant effect on the first reduction potential or quenching of the excited state by a sacrificial donor. Here, they tried to demonstrate the relation of the lifetime of one-electron reduction (OER) species and the dissociation of ligand X. The lifetime of the OER species is greatly reduced when X is a good leaving group. At low concentrations, complexes with the weakly bound ligand like Br^- have a short OER lifetime and does not show significant bimetallic interactions. On the other hand, at high concentrations, strongly bound ligands like NCS^- can show higher catalytic performance when the proximity of metal center is achieved through a covalent linkage, even though it has a short OER lifetime. In presence of a weakly bound ligand, the increased number of alkyl linkers have no effect on the catalytic activity, yet in the presence of bridging ligands to give a dinuclear complex, an increase in catalytic activity compared to the mononuclear complex is observed. They were able to successfully demonstrate that the adjustment of the proximity of two metal centers based on determining the lifetime of the OER intermediate follows a bimetallic pathway where the dinuclear rhenium complexes show higher photocatalytic performance as they can react more efficiently due to being covalently linked.

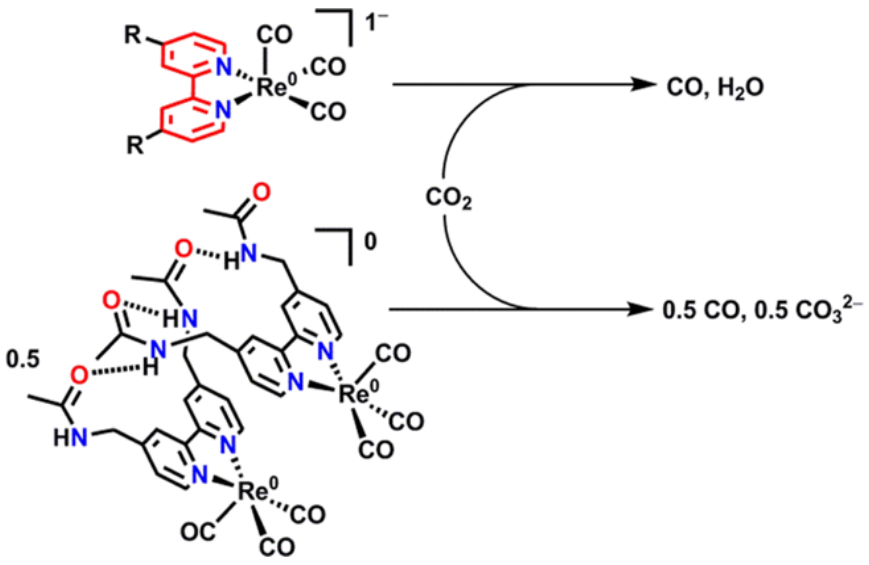

Figure 7. A dinuclear rhenium-based supramolecular assembly developed by the Kubiak Group which is accessed by hydrogen-bonding interactions *via* amide functionality.[16]

The Kubiak Group designed a supramolecular complex by the addition of methyl acetamidomethyl group at the 4,4'-position of a 2,2'-bipyridyl ligand, studied and compared their electrocatalytic activity with that of the model complex [(dmb)Re(CO)$_3$Cl].[16] The linkage of methyl acetamidomethyl groups was found to show an improved electrochemical behavior. Trifluoroethanol (TFE) was added as a proton source and shown to further enhance the catalytic activity. They carried out detailed studies on their supramolecular complex to account for the possible formation of a dimer in MeCN. Through infrared spectroelectrochemical (IR-SEC) studies, they were able to confirm the formation of a hydrogen bonded dimer by evaluating the lower shift in frequencies. They also performed IR-SEC studies to determine the co-products of CO_2 reduction which were found to be CO and CO_3^{2-}, suggestive of reductive disproportionation of CO_2. Though the formation of a dimer was theoretically determined to raise the potential due to the additional reduction process involved in the cleavage of metal-metal bonds, the CVs show that

the supramolecular complex performs CO_2 reduction at a much lower overpotential than the model complex $(dmb)Re(CO)_3Cl$.

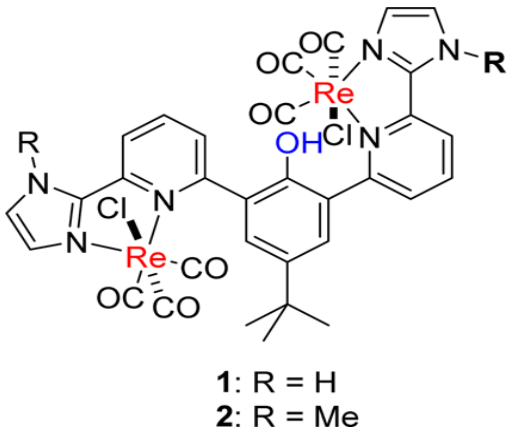

1: R = H
2: R = Me

Figure 8. Dinuclear rhenium complex with a phenolic proton relay at the bridge in close proximity to the metal center active sites, which was developed by the Siewert Group.[18]

The Siewert Group synthesized a dinuclear α-diimine rhenium complex with a proton responsive ligand (4-tert-butyl-2,6-bis(6-(1H-imidazol-2-yl)phenol) in close proximity to the metal center for studying the effect of a proton responsive ligand on electrochemical CO_2 reduction.[19] Through IR spectroscopy, they found that the H and Me substituted ligands have similar effects with both displaying a CO stretching frequency lower than the benchmark catalyst. CVs of the catalyst in DMF with added water displayed a slight shift in the second reduction peak with enhanced catalytic current at lower overpotentials with increasing concentrations of H_2O. This behavior is hypothesized to occur due to the catalyst favoring CO_2 reduction over OH-bond cleavage at the ligand. Higher catalytic activity of this dimeric complex having a proton responsive ligand in close proximity to the active metal center demonstrates that the bridging phenol can act as a proton relay and participate in the proton-coupled reduction of CO_2 during catalysis.

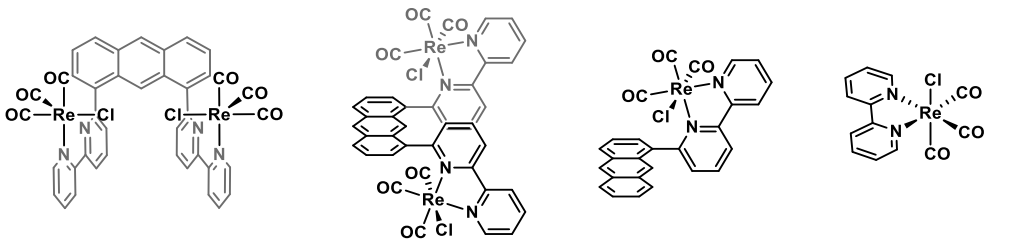

Figure 9. Mononuclear and dinuclear rhenium catalysts synthesized and studied by the Jurss Group.[7]

With relatively limited examples from the literature of dinuclear rhenium catalysts for CO_2 reduction as described above, the Jurss Group synthesized rigid mononuclear and dinuclear rhenium complexes bearing an anthracene chromophore, in which the rhenium active sites are held in close proximity in order to study the effects of one metal active site *versus* two and compared their electrocatalytic activity with the benchmark catalyst.[7] The dinuclear rhenium complex was found to have two isomeric forms, a symmetric *cis* conformer and an asymmetric *trans* conformer, as determined by NMR and IR spectroscopy. In electrochemical studies, the *cis* conformer (***cis*-Re_2Cl_2**) displayed a higher catalytic activity and was found to operate through a different mechanism for CO_2 reduction to CO compared to the *trans* conformer (***trans*-Re_2Cl_2**). Indeed, the ***cis*-Re_2Cl_2** catalyst displayed the highest catalytic activity with a turnover frequency (TOF) of 35.3 s^{-1}, the catalytic activity of the mononuclear catalyst were comparable to that of ***trans*-Re_2Cl_2** with a TOF of ~20 s^{-1}. All three catalysts were seen to outperform the benchmark catalyst $Re(bpy)(CO)_3Cl$ which had a TOF of 11.1 s^{-1} under the same conditions. This result show that two metal actives can be better than one, and that the pendant anthracene may also lead to improved catalysis. The mononuclear and dinuclear rhenium catalysts were investigated in the presence of different proton sources in order to explore their effect on electrocatalytic CO_2 reduction. It was

postulated that the symmetric structure of ***cis*-Re_2Cl_2** makes the orientation of the dinuclear complex suitable for a cooperative bimetallic pathway, which increases the catalytic rate for CO_2 reduction.

The anthracene-functionalized catalysts developed by the Jurss Group were further tested for their photocatalytic activity by collaboration with the Delcamp Group in the Department of Chemistry and Biochemistry at the University of Mississippi. One of the benefits of using rhenium-based catalysts for CO_2 reduction is that they are known to possess a unique property in which they can act as both the photosensitizer and CO_2 reducing catalyst. In the dinuclear systems, one metal center can act as a photosensitizer whereas the other can be used as the catalyst. Indeed, both ***cis*-** and ***trans*-Re_2Cl_2** were found to have a higher reactivity than the mononuclear catalysts as the two rhenium centers can cooperate efficiently by being covalently linked together. The di-rhenium catalysts performed significantly better (~4X higher TON) than the benchmark catalyst when the relative concentration of Re active sites was held constant. Despite the structural differences of ***cis*-Re_2Cl_2** and ***trans*-Re_2Cl_2**, the initial rates displayed by these catalysts were comparable to each other with both being faster (~6X higher TON) than the mononuclear complexes. A comparison of the anthracene-substituted monomer (**anthryl-Re**) with the benchmark catalyst $Re(bpy)(CO)_3Cl$ also shows that the anthracene itself actually has a negative impact on photocatalytic activity (**Figure 12**). This work is being communicated in the peer-reviewed literature and is currently under revision.

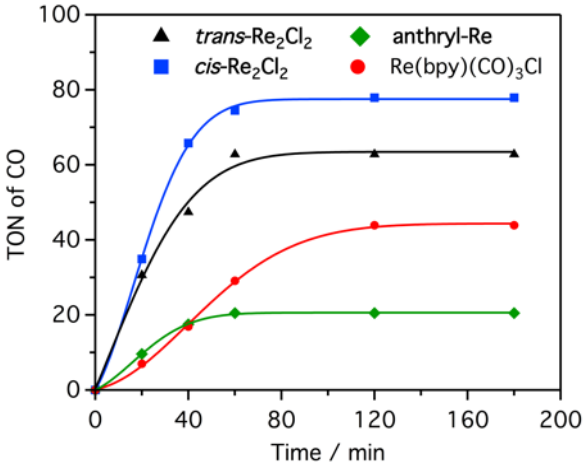

Figure 10. TON for CO production vs time for 0.1 mM ***cis*-Re_2Cl_2**, 0.1 mM ***trans*-Re_2Cl_2**, 0.2 mM **anthryl-Re**, and 0.2 mM $Re(bpy)(CO)_3Cl$.

Mechanism of Electrocatalytic CO_2 Reduction

From extensive mechanistic studies, $Re(bpy)(CO)_3X$-type catalysts are known to follow a single-site monometallic pathway during electrocatalysis where a catalyst in its initial state gets reduced by one-electron to form an anionic species. After the loss of chloride (or similar anionic monodentate ligand, X), a second reduction takes place to form the catalytically-active intermediate with an open coordination site for CO_2 activation. However, in certain cases, for example, in supramolecular assemblies or covalently-linked active sites or at relatively high catalyst concentrations, the catalyst can also operate through a competing bimetallic pathway.[16] In the bimetallic pathway, the one-electron reduced (OER) catalyst reacts with another OER catalyst to form a dimer (a dinuclear species containing a metal-metal bond), which gets reduced by one-electron to form the catalytically-active intermediate following metal-metal bond cleavage.

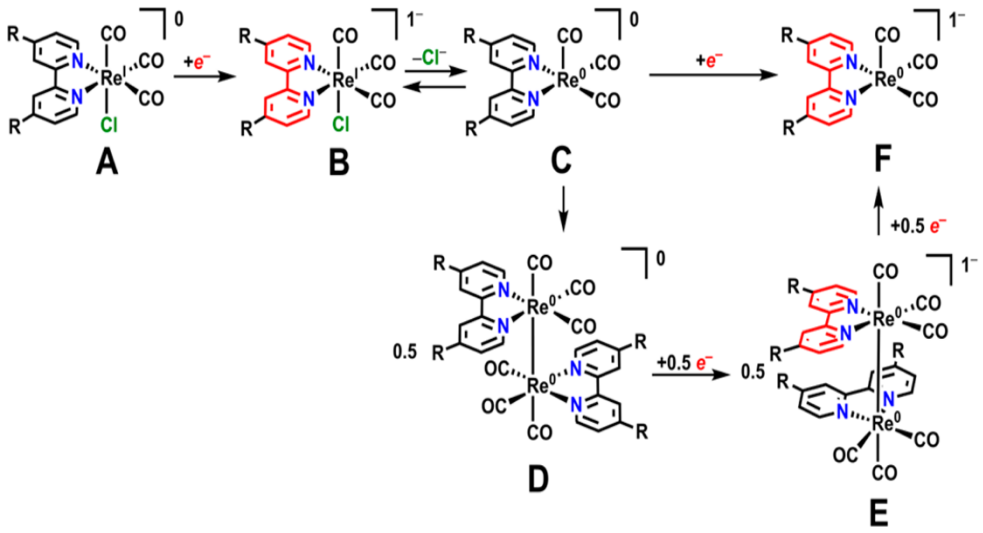

Figure 11. Mechanism for reduction of Re(bpy)(CO)$_3$X-type catalysts to form the catalytically-active intermediate (F) as proposed by Kubiak and coworkers.[16]

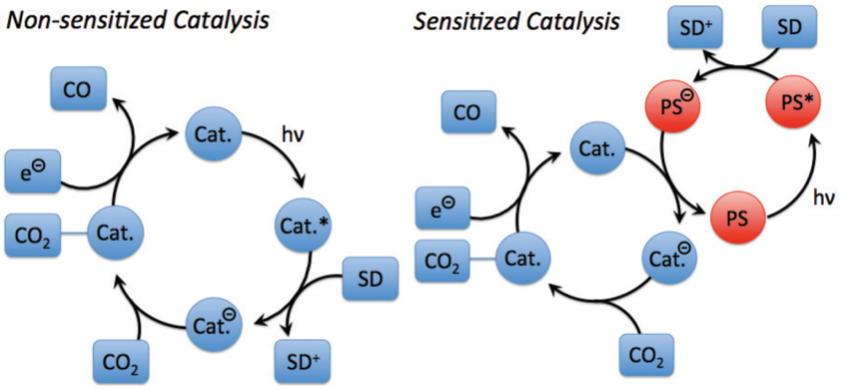

Figure 12. The effect of photosensitizer on a metal ligand complex for enhancement of CO_2 reduction.[19]

Under photocatalytic conditions with these catalysts, different mechanistic steps are observed and photosensitizers can have a substantial effect on the activity of the catalyst. Photosensitizers often have large delocalized π systems, which lowers the energy of LUMO orbitals.[20]

Photocatalytic CO_2 reduction can be performed in two ways. In a sensitized catalytic cycle, photosensitizers are activated by a photon source first and then reduced by excited state quenching with a sacrificial electron donor molecule. The catalyst gets reduced by the reduced photosensitizer molecule, which subsequently can react with carbon dioxide. Upon the addition of a second electron in the system, the reduced catalyst reduces CO_2 to CO and regenerates the catalyst as illustrated in **Figure 6.** In a non-sensitized catalytic cycle, light excites the catalyst, which then gets reduced by the sacrificial electron donor before it can activate carbon dioxide. Upon the addition of a second electron in the system, the reduced catalyst reduces CO_2 to CO and regenerates the catalyst. In a sensitized photocatalysis, an external photosensitizer such as *fac*-Ir(ppy)$_3$ needs to be employed for the activation of the complex for CO_2 reduction whereas in a non-sensitized photocatalysis, the catalyst itself serves as a photosensitizer for light absorption and CO_2 reduction.

One of the main benefits of using the anthracene-based polypyridyl ligand in our complex is that these catalysts possess a long-lived excited triplet state. When appropriate light is shined on the complex bearing a pendent anthracene, the electrons get excited to its higher energy state where metal-to-ligand charge transfer (^{1}MLCT) takes place. Since rhenium is a heavy metal and has significant spin-orbit coupling, intersystem crossing occurs to generate the triplet MLCT excited state which is lower in energy. This excited state continues to be funneled downhill to an anthracene-based triplet excited state that is exceptionally long-lived as the transition from the triplet organic chromophore back to the singlet ground state is a spin forbidden process without the benefit of significant spin-orbit coupling. The long-lived excited state facilitates reductive quenching with a sacrificial donor, such as BIH, and makes photocatalysis more efficient. These basic photophysical processes and their relative energies are shown in **Figure 15**.

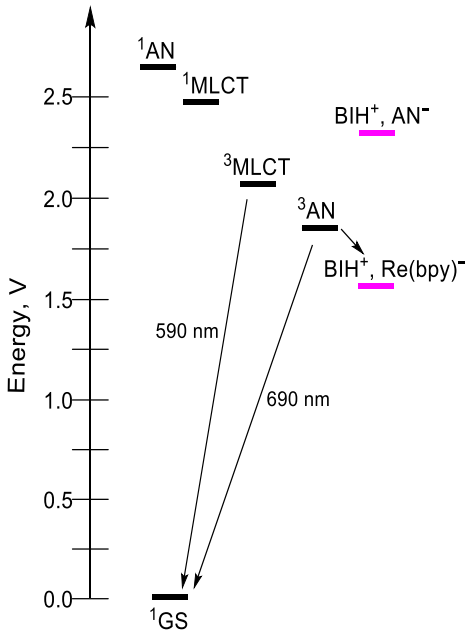

Figure 13. Excited state energetics and reaction with sacrificial donor BIH to form a reduced anthracene-functionalized rhenium species.

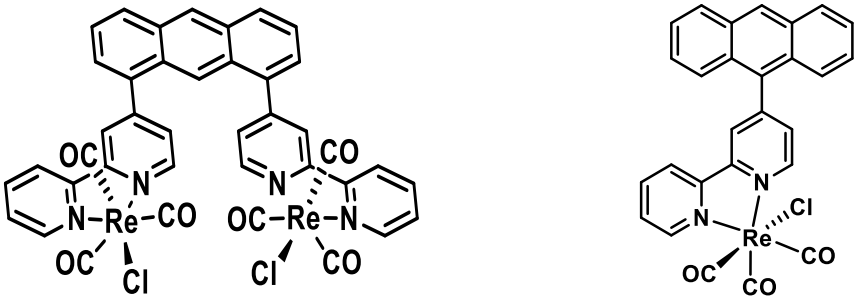

Figure 14. Mononuclear and dinuclear rhenium catalysts synthesized and studied in this work.

It has been previously reported in literature that extending the π framework by making the polypyridyl ligand coplanar to rigid anthracene moiety increased the lifetime of anthracene excited state. Enhancing the lifetime of triplet state theoretically should have a positive impact of the photochemical performance of this type of catalysts. By this work, we wanted to see how a

coplanar and freely rotating mononuclear and dinuclear Re catalysts works for catalytic CO_2 reduction.

Results and Discussion

Synthetic routes for preparing the mononuclear (**1f**) and dinuclear (**2d**) rhenium catalysts containing a pendant anthracene functional group that can be coplanar with the bipyridine are shown below in **Synthetic Schemes 1** and **2**. Detailed procedures, characterization of the intermediates and final complexes, and associated references can be found in the Experimental section of the Supplemental Information.[7, 21-26]

Synthetic Scheme 1

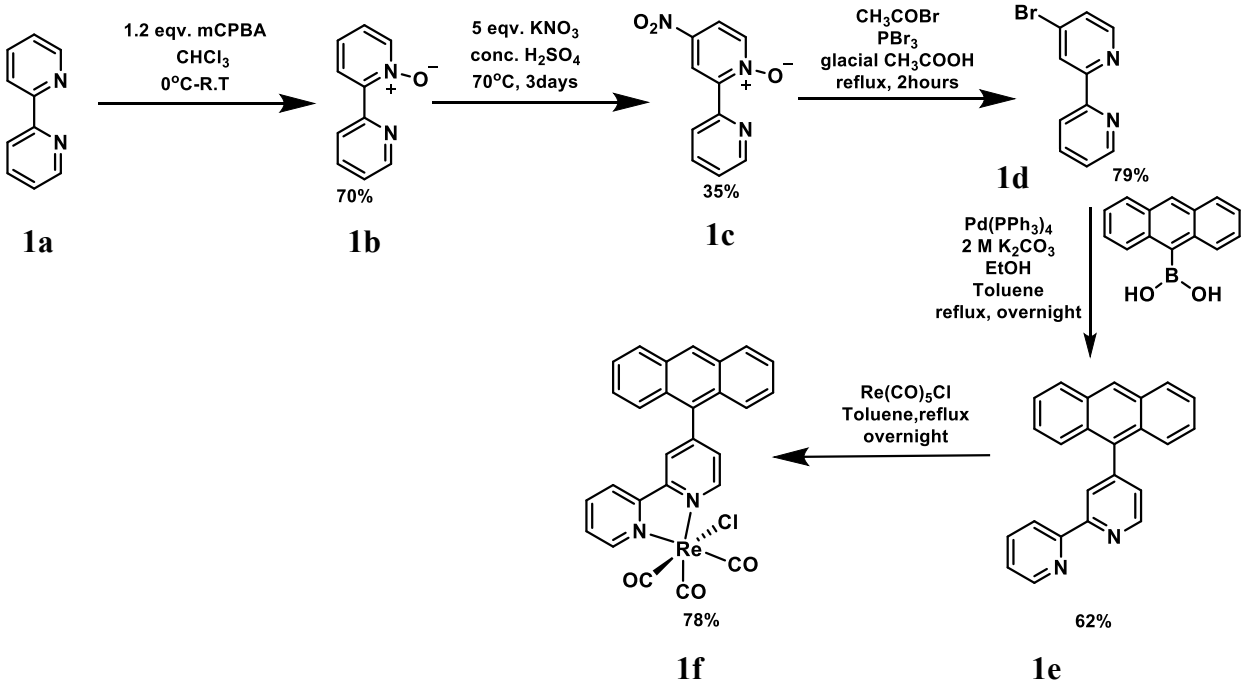

Synthetic Scheme 2

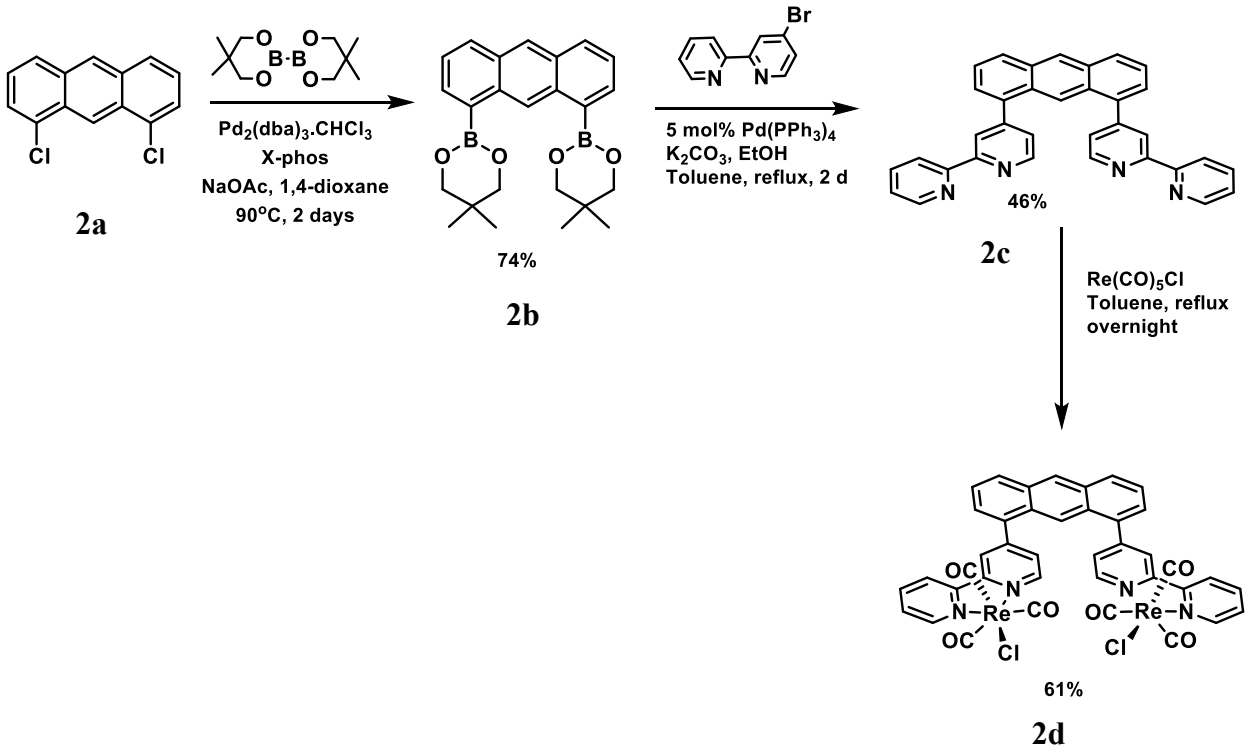

Materials and methods

All the synthetic procedures were performed in an inert atmosphere using standard Schlenk techniques unless otherwise mentioned. Toluene was dried with a Pure Process Technology solvent purification system. Anhydrous *N,N*-dimethylformamide (DMF) was purchased from Alfa Aesar packed under argon. The rhenium precursor $Re(CO)_5Cl$ was purchased from Stream and stored in a glovebox. All other chemicals were reagent or ACS-grade, purchased from commercial vendors and used without further purification. All the NMRs (^1H and ^{13}C) were obtained using a Bruker Advance DRX-500 spectrometer operating at 500 MHz (^1H) and 126 MHz (^{13}C). Thin-layer chromatography was done on Sigma T-6145 pre-coated TLC Silica gel polyester sheets which was visualized using UV lamps. The deactivated silica column was made by using (100:1) MeOH:TEA (triethylamine). All chemical shifts are reported in ppm. The *cis* and *trans* isomers

could not be separated for our dinuclear catalyst. Hereafter, the mixture of *cis* and *trans* isomers were subjected for further investigation.

Photocatalysis

Photocatalytic experiments were performed with a 150 W Science tech SF-150C Small Collimated Beam Solar Stimulator equipped with an AM 1.5 filter. The conditions employed for all experiments involved 0.1 mM catalyst, 10 mM 1,3-dimethyl-2-phenyl-2*H*-benzimidazole (BIH), and 5% triethylamine (TEA) in stirred CO_2-saturated solutions of either MeCN or DMF as specified. Headspace analysis was performed using a gas tight syringe with stopcock and Agilent 7890B Gas Chromatograph. Quantitation of CO was made using an FID detector whereas H_2 was quantified using a TCD detector. Calibration was done using the standards purchased from buycalgas.com.

Table 2: TON of CO displayed by the mononuclear rhenium complex (catalyst **1f**) in MeCN and DMF at different time intervals.

Time (hr)	TON_{CO} (MeCN)	TON_{CO} (DMF)
0.33	35	3.5
0.66	84	10
1	111	17
2	127	29
4	130	32

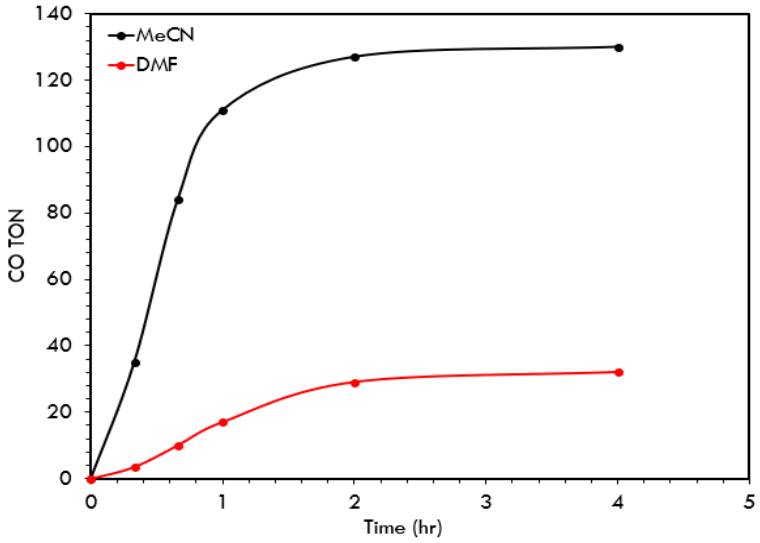

Figure 15. TON for CO production vs time for 0.1 mM mononuclear Re complex (**1f**) in MeCN and DMF solutions. This data was collected by Shakeiya Davis.

Table 2 and **Figure 15** illustrates the effect of different solvent system on the photocatalytic activity of the metal complexes. This illustrates that the performance in MeCN is almost 5 times better than that in DMF.

Table 3. Comparison of TON of evolved CO by mononuclear and dinuclear Re catalysts in MeCN.

Catalyst	TON
Mononuclear (**1f**)	109
Dinuclear (**2d**)	159

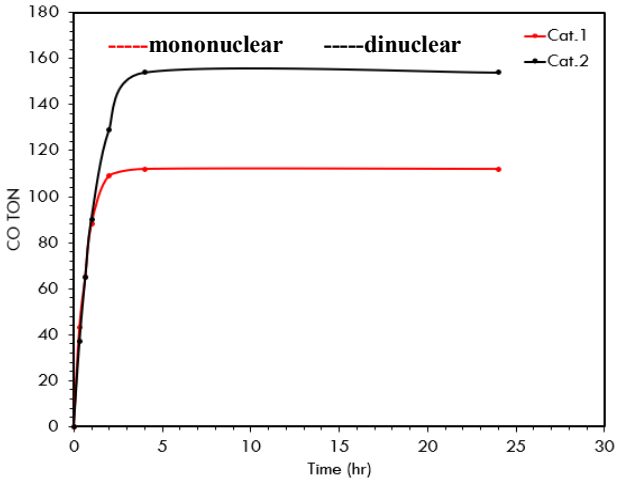

Figure 16. TON for CO production for 0.1 mM mononuclear (**1f**) and dinuclear (**2d**) Re catalysts in MeCN solutions containing BIH and TEA. Data collected by Shakeiya Davis.

After the mononuclear catalyst was determined to show a greater durability and performance in MeCN, we compared the TON for CO for both of our catalysts in MeCN. **Table 3** shows that the TON for the dinuclear complex is greater than that of the mononuclear complex. **Figure 16** also shows that both of our catalysts are active for a long period of time. Higher TON for the dinuclear catalyst **2d** is consistent with the hypothesis that the presence of two metal centers enables more efficient accumulation of reducing equivalents for improved CO_2 conversion.[25] A photosensitizer pathway can be generally used to describe this difference in TON between the mononuclear and dinuclear rhenium complexes. In the dinuclear Re_2Cl_2 system (**2d**), the catalyst functions through an intramolecular pathway in which one rhenium complex acts as a photosensitizer and the other acts as both photocatalyst and electrocatalyst. The durability of such complexes is thought to arise from a shorter lifetime of the one-electron reduced intermediates as photocatalysis is more efficient with two metal center covalently linked.[26]

Electrocatalysis

Electrochemistry was performed with a Bioanalytical Systems, Inc. (BASi) Epsilon potentiostat. A three-electrode cell employing a glassy carbon disk (3 mm dia.) working electrode, a platinum wire counter electrode, and a silver wire quasi-reference electrode was used for the cyclic voltammetry studies. Cyclic voltammetry was employed to study the turnover frequencies (TOF). Controlled potential electrolysis was employed to study the efficiency and life span of the metal complex. Electrochemistry was conducted in anhydrous DMF and MeCN containing 0.1 M tetrabutylammonium hexafluorophosphate ($TBAPF_6$) supporting electrolyte. Solutions were degassed thoroughly with argon or carbon dioxide for at least 30 min before collecting data and all cyclic voltammograms (CVs) were started at the most positive potential and cycled through the most negative potential and back. Ferrocene was added at the end of experiments as an internal standard to reference the potential.

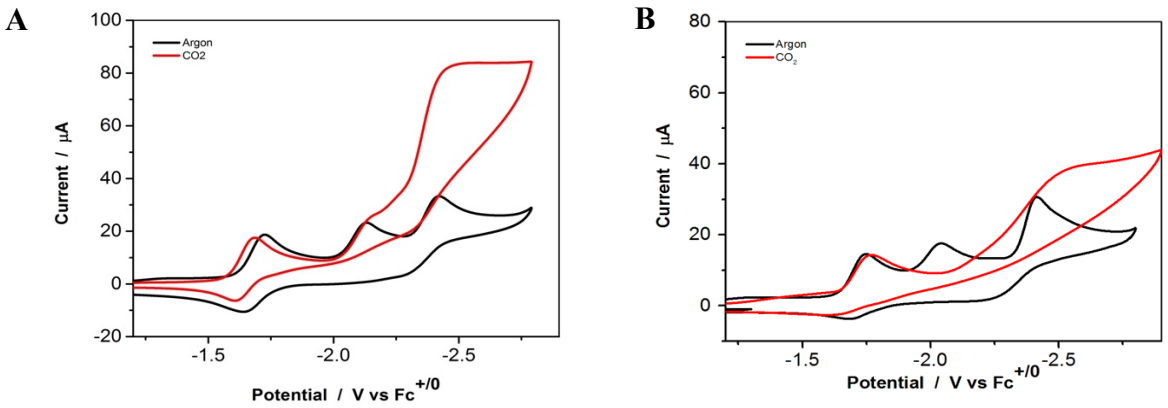

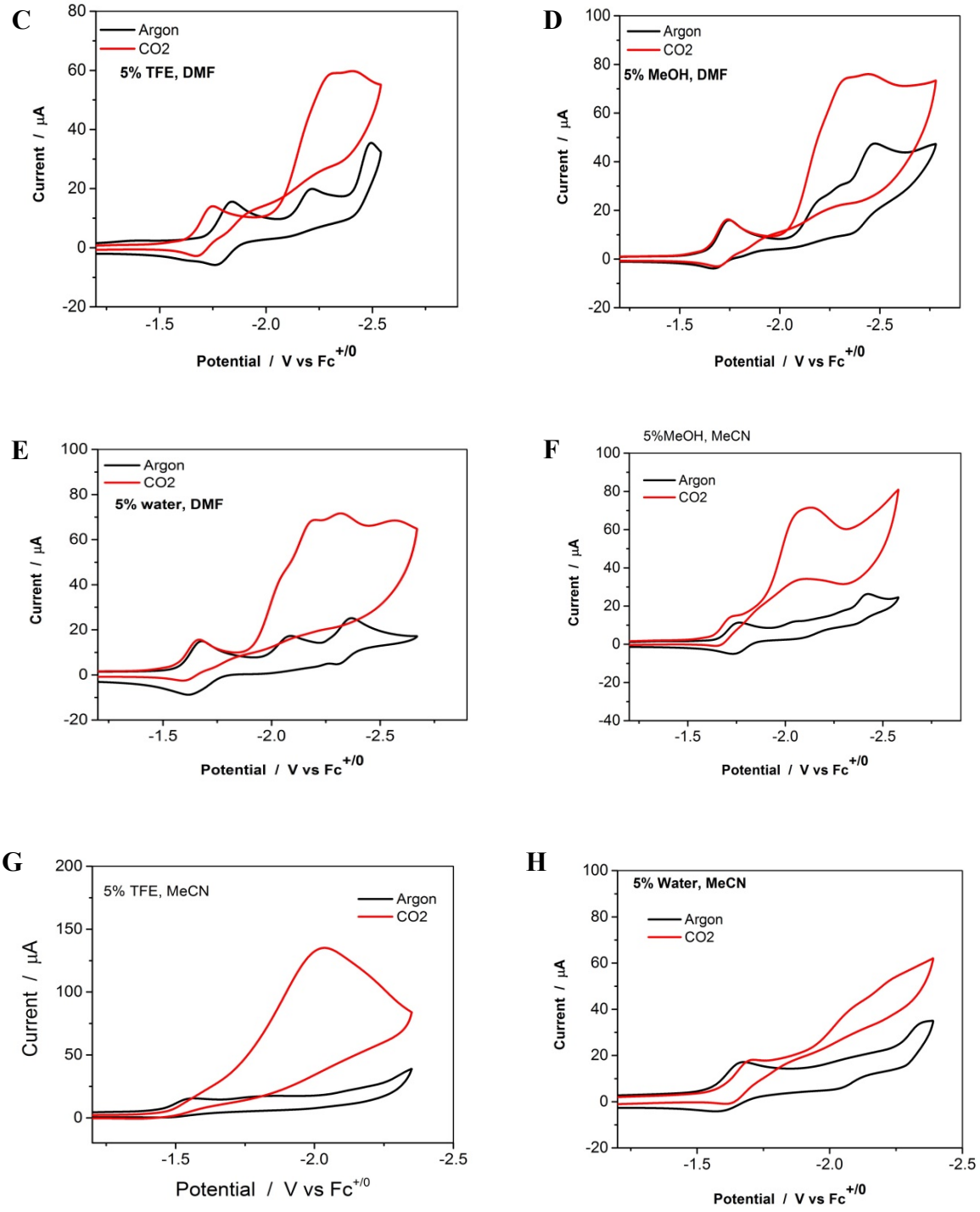
C
Argon
CO2
5% TFE, DMF
Current / µA
Potential / V vs Fc+/0
D
Argon
CO2
5% MeOH, DMF
Current / µA
Potential / V vs Fc+/0
E
Argon
CO2
5% water, DMF
Current / µA
Potential / V vs Fc+/0
F
5%MeOH, MeCN
Argon
CO2
Current / µA
Potential / V vs Fc+/0
G
5% TFE, MeCN
Argon
CO2
Current / µA
Potential / V vs Fc+/0
H
5% Water, MeCN
Argon
CO2
Current / µA
Potential / V vs Fc+/0

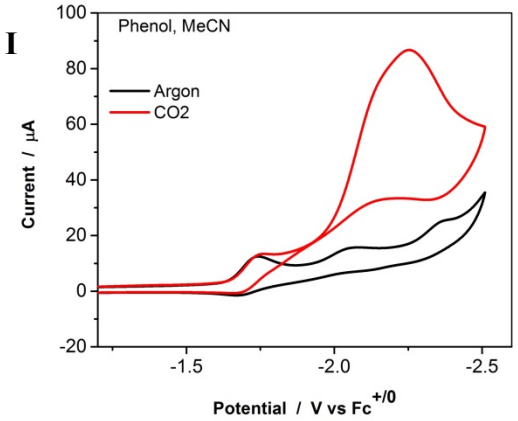

Figure 17. CVs of 0.5 mM mononuclear Re complex (**1f**) under Ar (black) and CO_2 (red) in 0.1 M $TBAPF_6$/(DMF or MeCN) using different proton sources. (**A**-DMF, **B**-MeCN, **C**-DMF-5% TFE, **D**-DMF-5% MeOH, **E**-DMF-5% H_2O, **D**-MeCN-5% TFE, **G**-MeCN-5% MeOH, **H**-MeCN-5% H_2O, **I**-MeCN-Phenol).

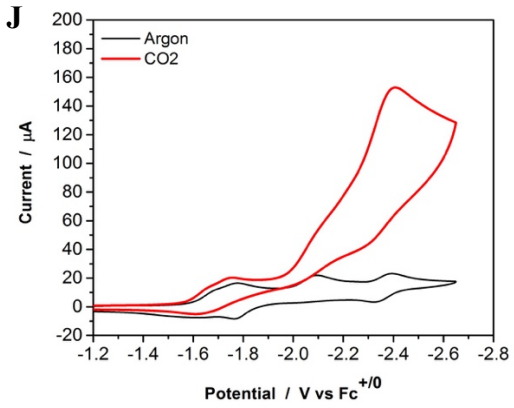

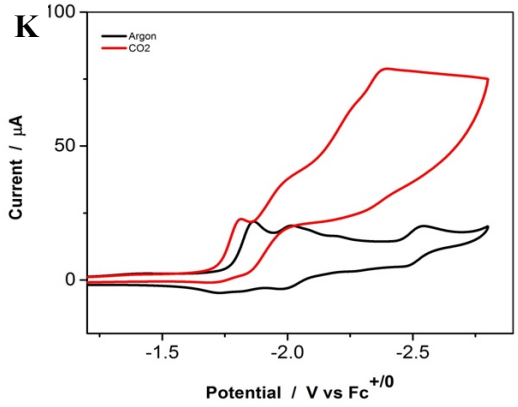

L

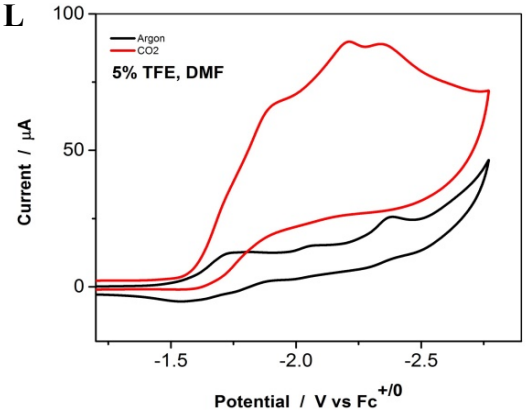
Argon
CO2
5% TFE, DMF
Current / µA
Potential / V vs Fc+/0

M

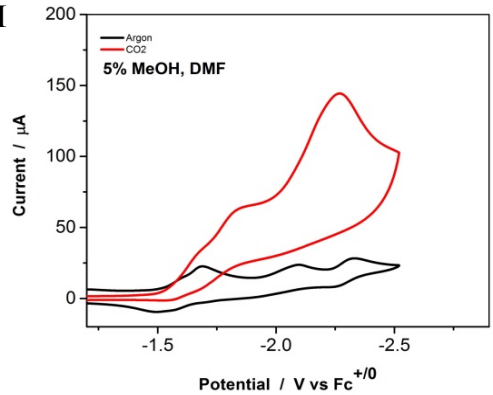
Argon
CO2
5% MeOH, DMF
Current / µA
Potential / V vs Fc+/0

N

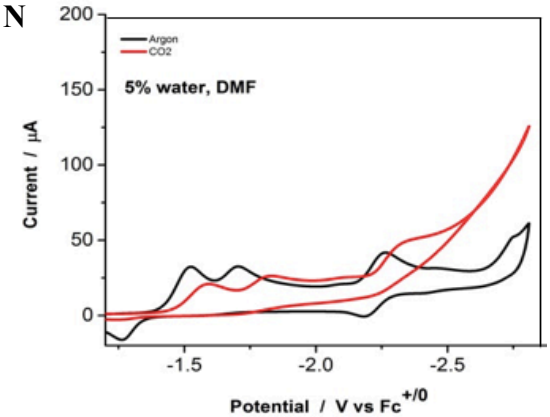
Argon
CO2
5% water, DMF
Current / µA
Potential / V vs Fc+/0

O

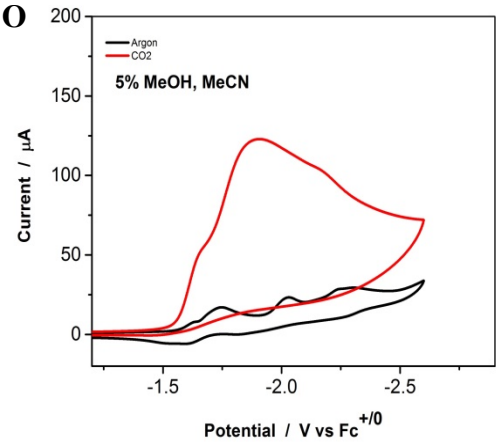
Argon
CO2
5% MeOH, MeCN
Current / µA
Potential / V vs Fc+/0

P

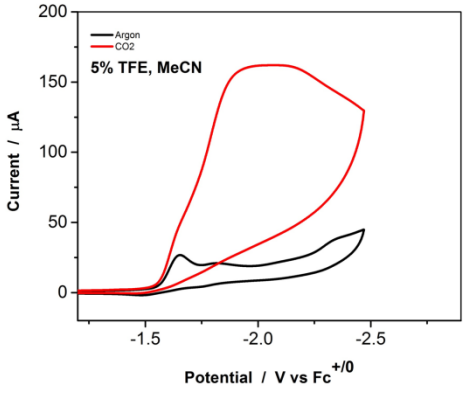
Argon
CO2
5% TFE, MeCN
Current / µA
Potential / V vs Fc+/0

Q

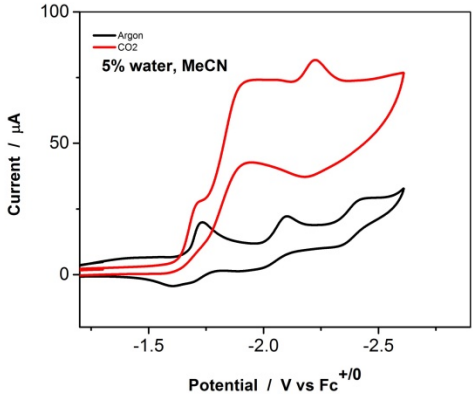
Argon
CO2
5% water, MeCN
Current / µA
Potential / V vs Fc+/0

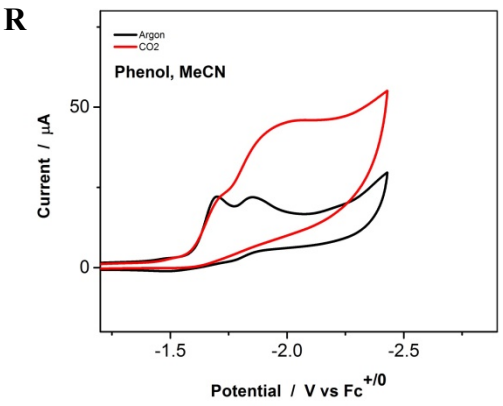

Figure 18. CVs of 0.5 mM dinuclear rhenium complex (**2d**) under Ar (black) and CO_2 (red) in 0.1 M $TBAPF_6$/(DMF or MeCN) using different proton sources. (**J**-DMF, **K**-MeCN, **L**-DMF-5% TFE, **M**-DMF-5% MeOH, **N**-DMF-5% H_2O, **O**-MeCN-5% TFE, **P**-MeCN-5% MeOH, **Q**-MeCN-5% H_2O, **R**-MeCN-Phenol).

Both the mononuclear (**1f**) and the dinuclear (**2d**) rhenium complexes were subjected to cyclic voltammetry under of argon and catalytic conditions (under CO_2), separately. From the cyclic voltammograms under argon, we can see three reduction peaks for the mononuclear complex in absence of any proton sources. The first and the most positive peak represents a ligand-based reduction, the middle peak represents metal-based reduction, and the third and most negative peak represents an anthracene-based reduction on the basis of an earlier report.[7] All of the data represented in the table below are directly derived from the CVs presented in **Figures 17** and **18**.

Table 4. CO_2 reduction potentials and (i_{cat}/i_p) values at second reduction peak of the mononuclear catalyst **1f** from cyclic voltammetry in anhydrous DMF/0.1 M Bu_4NPF_6 solutions.

Proton Source	**$E_{p,c}$**	**i_{cat}/i_p**

None	-2.46	2.87
5% TFE	-2.32	3.12
5% MeOH	-2.43	2.67
5% H_2O	-2.22	3.98

The mononuclear catalyst **1f** was investigated with DMF in presence of different common proton sources. The comparison can be seen in **Table 4.** The catalyst showed no significant changes in activity when the proton sources were introduced.

Table 5. CO_2 reduction potentials and (i_{cat}/i_p) values at second reduction peak of the dinuclear catalyst **2d** from cyclic voltammetry in anhydrous DMF/0.1 M Bu_4NPF_6 solutions.

Proton Source	$\mathbf{E_{p,c}}$	$\mathbf{i_{cat}/i_p}$
None	-2.38	7.45
5% TFE	-2.37	5.92
5% MeOH	-2.32	6.09
5% H_2O	-2.26	1.15

The dinuclear catalyst **2d** was investigated with DMF in presence of different common proton sources. The comparison can be seen in **Table 5.** The catalyst showed detrimental catalytic activity when the proton sources were introduced. Compared to the mononuclear Re complex, the dinuclear Re complex displayed a higher catalytic activity which can be explained in terms of the presence of two active metal sites versus one.

Table 6. CO_2 reduction potentials and (i_{cat}/i_p) values at second reduction peak of the mononuclear catalyst **1f** from cyclic voltammetry in anhydrous MeCN/0.1 M Bu_4NPF_6 solutions.

Proton Source	$\mathbf{E_{p,c}}$	$\mathbf{i_{cat}/i_p}$
None	-2.52	1.17
5% TFE	-2.08	5.94
5% MeOH	-2.10	5.22
5% H_2O	-2.04	2.14
5% Phenol	-2.32	4.66

The mononuclear catalyst **1f** was investigated with MeCN in presence of different common proton sources. The comparison can be seen in **Table 6.** The catalyst showed a significant increase the catalytic activity when the proton sources were introduced at a reduced catalytic potential value.

Table 7. CO_2 reduction potentials and (i_{cat}/i_p) values at second reduction peak of the dinuclear catalyst **2d** from cyclic voltammetry in anhydrous MeCN/0.1 M Bu_4NPF_6 solutions.

Proton Source	$\mathbf{E_{p,c}}$	$\mathbf{i_{cat}/i_p}$
None	-2.35	3.82
5% TFE	-1.82	7.80
5% MeOH	-1.88	5.26
5% H_2O	-1.91	3.32
5% Phenol	-1.84	2.04

The dinuclear catalyst **2d** was investigated with MeCN in presence of different common proton sources. The comparison can be seen in **Table 7.** The catalyst showed higher activity when the proton sources (5% TFE and 5% MeOH) were introduced. While, the catalytic activity decreased with other added proton sources, it is important to note the decrease in catalytic potentials too. Compared to the mononuclear Re complex, the dinuclear Re complex displays a higher catalytic activity in presence of 5% TFE.

Scan rate dependent cyclic voltammetry in DMF (Mononuclear complex **1f**)

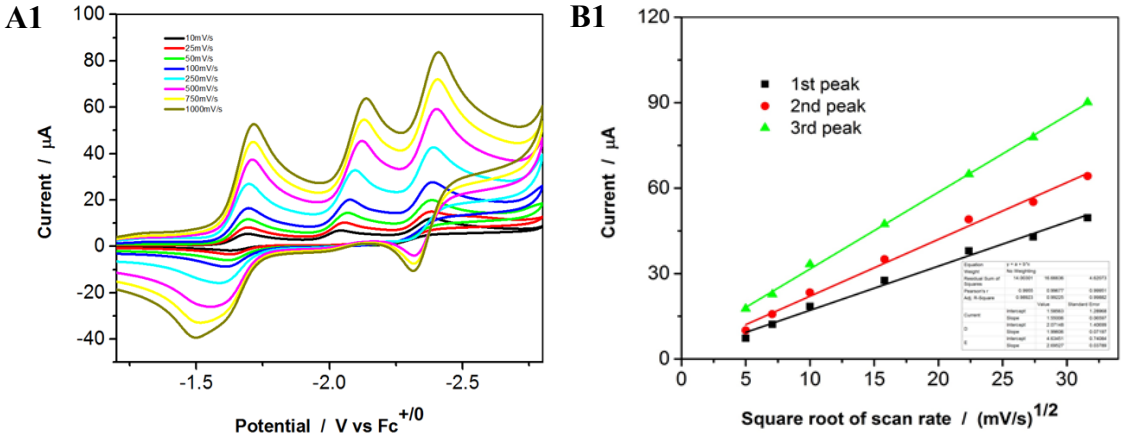

Scan rate dependent cyclic voltammetry in MeCN (Mononuclear complex **1f**)

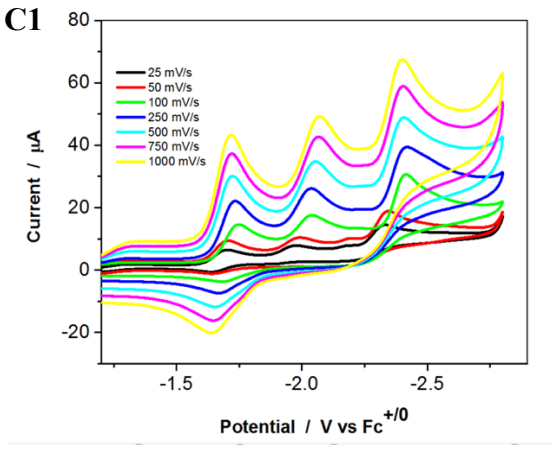

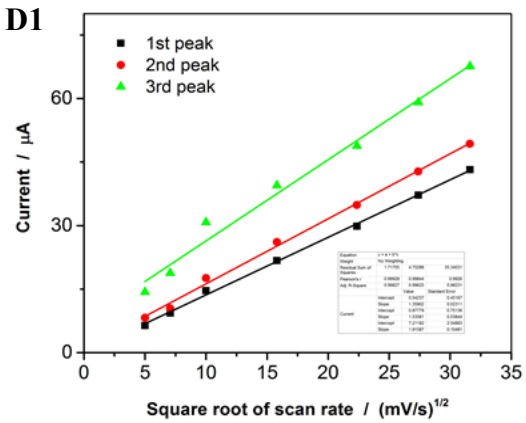

Scan rate dependent cyclic voltammetry in DMF (Dinuclear complex **2d**)

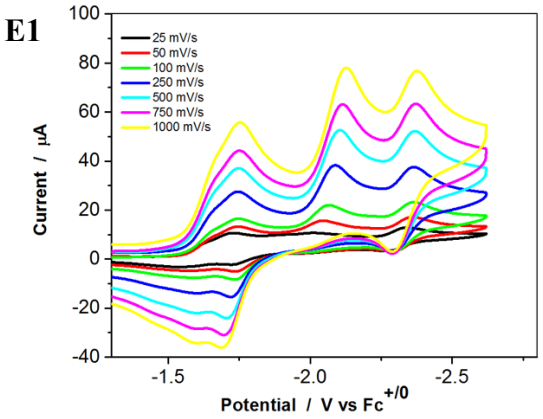

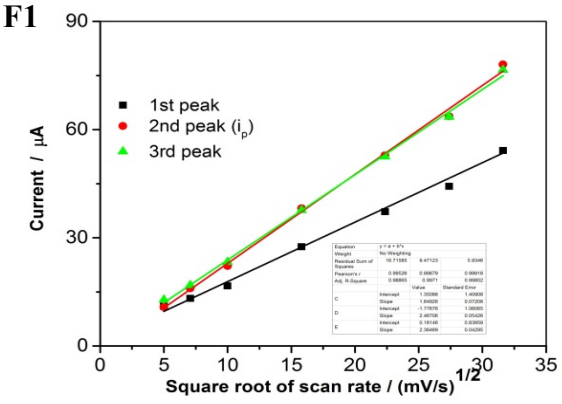

Scan rate dependent cyclic voltammetry in MeCN (Dinuclear complex **2d**)

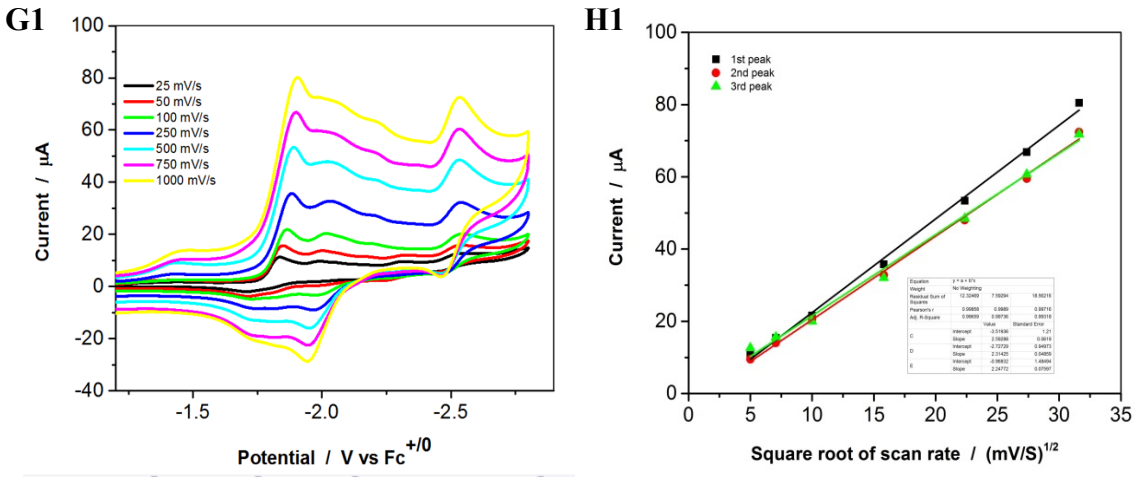

Figure 19. Mononuclear and dinuclear rhenium complexes: Cyclic voltammograms at different scan rates with 0.5 mM rhenium complexes under Ar atmosphere in DMF or MeCN solutions, as indicated, containing 0.1 M $TBAPF_6$. The scan rate dependence is shown next to each series of cyclic voltammograms in the plot of current (µA) versus the square root of the scan rate ($(mV/s)^{1/2}$). A linear fit is observed which confirms that the systems are homogeneous and diffusion controlled.

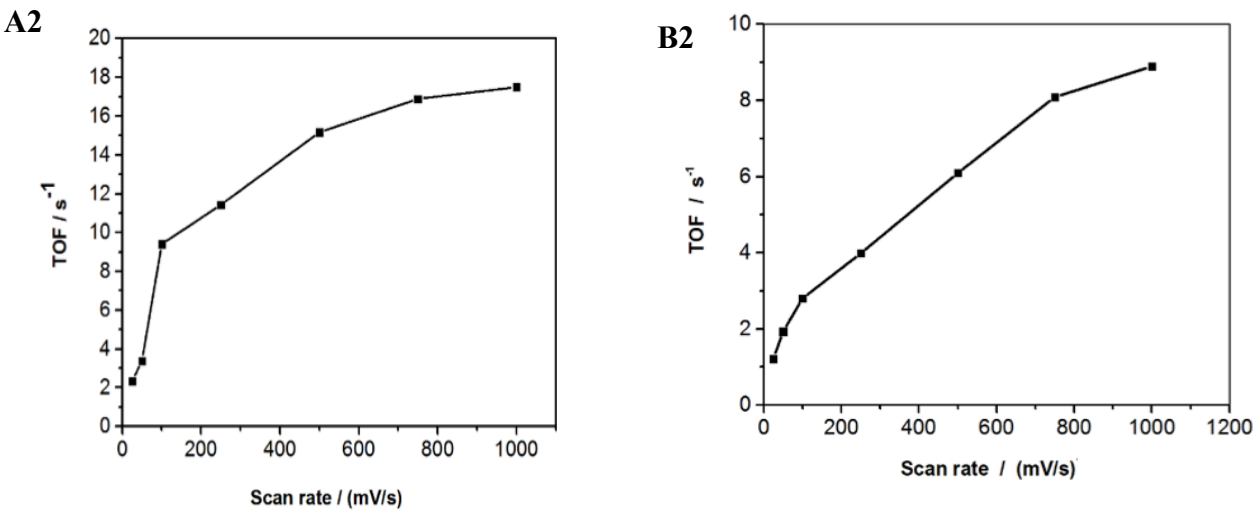

Figure 20. Representative TOF versus scan rate graph for dinuclear complex **2d** in DMF (**A2**), MeCN (**B2**).

Table 8. Summary of electrocatalysis obtained from cyclic voltammetry in DMF solutions.

Catalyst	TOF (s^{-1}) (DMF)
mononuclear-ReCl (**1f**)	17.3
dinuclear-Re_2Cl_2 (**2d**)	17.8
***cis*-Re_2Cl_2**	35.3
***trans*-Re_2Cl_2**	22.9
anthryl-Re	19.2

Table 9. Summary of electrocatalysis obtained from cyclic voltammetry in MeCN solutions.

Catalyst	TOF (s^{-1}) in MeCN
mononuclear-ReCl (**1f**)	5.9
dinuclear-Re_2Cl_2 (**2d**)	9.2

Electrochemistry was performed on both of our metal complexes to test for catalytic properties. The catalytic system was found to be diffusion controlled. From the cyclic voltammograms of the complexes in different solvents and with different added proton sources, MeCN with 5% TFE was found to produce the highest catalytic current in CO_2-saturated solutions with both the mononuclear (**1f**) and dinuclear (**2d**) catalysts. After calculations were performed to determine turnover frequencies (TOF), the TOFs were plotted versus the scan rate to obtain maximum scan rate independent TOF values (as shown in **Figure 20**). Since our metal complexes were soluble in both DMF and MeCN, we wanted to study the catalytic activity in these two different solvents. The results show that our metal complex is more catalytically active in DMF solutions in comparison to MeCN. The TOFs obtained for both the mononuclear and dinuclear Re_2Cl_2 complexes in DMF (~18 s^{-1}) are comparable to the TOFs of the previously reported catalysts with TOFs of ***trans*-Re_2Cl_2** (22.9 s^{-1}) and **anthryl-Re** (19.2 s^{-1}).[7]

Conclusions

We have synthesized and studied novel polypyridyl mononuclear and dinuclear rhenium complexes containing a pendant anthracene chromophore. The catalytic rates were measured by cyclic voltammetry for mononuclear- and dinuclear rhenium catalysts (**1f** and **2d**, respectively) with estimated TOFs of 17.3 and 17.8 s^{-1}, respectively. The TOFs obtained for both the mononuclear and dinuclear Re catalysts in DMF (~18 s^{-1}) are comparable to the TOFs of related and previously reported systems which had measured TOFs for ***trans*-Re_2Cl_2** (22.9 s^{-1}) and **anthryl-Re** (19.2 s^{-1}).[7] Results obtained from the electrochemistry and photocatalysis data confirm that both of our catalysts show notable activity for CO_2 reduction. Photocatalysis data show that our catalysts are very active with higher TONs of 109 and 159 for the mononuclear and dinuclear rhenium complexes, respectively. When compared with the TON results of the previously studied rigid mononuclear and dinuclear complexes (TONs as high as ~80), the photocatalytic activity displayed by our second-generation catalysts (**1f** and **2d**) are comparatively higher which demonstrates that an unhindered rotation has a positive impact on the photocatalytic activity, consistent with our initial hypothesis. Both mononuclear (**1f**) and dinuclear (**2d**) Re complexes show a higher catalytic activity in MeCN in presence of 5% TFE. Some of the future works include obtaining better ^{13}C NMRs, obtaining Faradaic efficiencies for the dinuclear-Re_2Cl_2 (**2d**) complex, and establishing a procedure to separate the *cis* and *trans* isomers in order to compare their electrocatalytic and photocatalytic performances for CO_2 reduction.

References

(1) A First Course in Atmospheric Radiation – G.W. Petty http://sundogpublishing.com/products/a-first-course-in-atmospheric-radiation-g-w-petty (accessed Nov 2, 2018).

(2) Bennett (NOAA), J. Ocean Acidification http://ocean.si.edu/ocean-life/invertebrates/ocean-acidification (accessed Nov 2, 2018).

(3) User, S. Daily CO_2 https://www.co2.earth/daily-co2 (accessed Nov 2, 2018).

(4) EIA projects world energy consumption will increase 56% by 2040 - Today in Energy - U.S. Energy Information Administration (EIA) https://www.eia.gov/todayinenergy/detail.php?id=12251(accessed Nov 2, 2018).

(5) U.S. Energy Information Administration (EIA) - Total Energy Monthly Data https://www.eia.gov/totalenergy/data/monthly/ (accessed Nov 2, 2018).

(6) Barber, J.; Tran, P. D. From Natural to Artificial Photosynthesis. *Soc. Interface* **2013**, *10* (81).

(7) Yang, W.; Sinha Roy, S.; Pitts, W. C.; Nelson, R. L.; Fronczek, F. R.; Jurss, J. W. Electrocatalytic CO_2 Reduction with *Cis* and *Trans* Conformers of a Rigid Dinuclear Rhenium Complex: Comparing the Monometallic and Cooperative Bimetallic Pathways. *Inorg. Chem.* **2018**, *57*(15), 9564–9575.

(8) Steinberg-Yfrach, G.; Liddell, P. A.; Hung, S. C.; Moore, A. L.; Gust, D.; Moore, T. A. Conversion of Light Energy to Proton Potential in Liposomes by Artificial Photosynthetic Reaction Centres. *Nature* **1997**, *385* (6613), 239–241.

(9) Steinberg-Yfrach, G.; L Rigaud, J.; Durantini, E.; Moore, A.; Gust, D.; Moore, T. Light-Driven Production of ATP Catalysed by F0F1-ATP Synthase in an Artificial Photosynthetic Membrane. *Nature* **1998**, *392*, 479–482.

(10) Robert, M. Proton-Coupled Electron Transfer. *Energy Environ. Sci.* **2012**, *5* (7), 7695–7695.

(11) Finn, C.; Schnittger, S.; Yellowlees, L. J.; Love, J. B. Molecular Approaches to the Electrochemical Reduction of Carbon Dioxide. *Chem. Commun.* **2012**, *48* (10), 1392–1399.

(12) Benson, E. E.; Kubiak, C. P.; Sathrum, A. J.; Smieja, J. M. Electrocatalytic and Homogeneous Approaches to Conversion of CO_2 to Liquid Fuels. *Chem. Soc. Rev.* **2009**, *38* (1), 89–99.

(13) Nikparsa, P.; Mirzaeia, A. A.; Atashi, H. Effect of Reaction Conditions and Kinetic Study on the Fischer-Tropsch Synthesis over Fused Co-Ni/Al_2O_3 Catalyst. *J. Fuel Chem. Technol.* **2014**, *42*, 710–718.

(14) Sakakura, T.; Choi, J.-C.; Yasuda, H. Transformation of Carbon Dioxide. *Chem. Rev.* **2007**, *107* (6), 2365–2387.

(15) Liyanage, N. P.; Dulaney, H. A.; Huckaba, A. J.; Jurss, J. W.; Delcamp, J. H. Electrocatalytic Reduction of CO_2 to CO With Re-Pyridyl-NHCs: Proton Source Influence on Rates and Product Selectivities. *Inorg. Chem.* **2016**, *55* (12), 6085–6094.

(16) Machan, C. W.; Chabolla, S. A.; Yin, J.; Gilson, M. K.; Tezcan, F. A.; Kubiak, C. P. Supramolecular Assembly Promotes the Electrocatalytic Reduction of Carbon Dioxide by Re(I) Bipyridine Catalysts at a Lower Overpotential. *J. Am. Chem. Soc.* **2014**, *136* (41), 14598–14607.

(17) Bruckmeier, C.; Lehenmeier, M. W.; Reithmeier, R.; Rieger, B.; Herranz, J.; Kavakli, C. Binuclear Rhenium(I) Complexes for the Photocatalytic Reduction of CO_2. *Dalton Trans.* **2012**, *41* (16), 5026–5037.

(18) Wilting, A.; Stolper, T.; Mata, R. A.; Siewert, I. Dinuclear Rhenium Complex with a Proton Responsive Ligand as a Redox Catalyst for the Electrochemical CO_2 Reduction. *Inorg. Chem.* **2017**, *56* (7), 4176–4185.

(19) Huckaba, A. J.; Sharpe, E. A.; Delcamp, J. H. Photocatalytic Reduction of CO_2 with Re-Pyridyl-NHCs. *Inorg. Chem.* **2016**, *55* (2), 682–690.

(20) Schindler, J.; Zhang, Y.; Traber, P.; Lefebvre, J.-F.; Kupfer, S.; Demeunynck, M.; Gräfe, S.; Chavarot-Kerlidou, M.; Dietzek, B. A Ππ* State Enables Photoaccumulation of Charges on a π-Extended Dipyridophenazine Ligand in a Ru(II) Polypyridine Complex. *J. Phys. Chem. C* **2018**, *122* (1), 83–95.

(21) Wada, T.; Muckerman, J. T.; Fujita, E.; Tanaka, K. Substituents Dependent Capability of Bis(Ruthenium-Dioxolene-Terpyridine) Complexes toward Water Oxidation. *Dalton Trans.* **2011**, *40* (10), 2225–2233.

(22) Egbe, D. A. M.; Amer, A. M.; Klemm, E. Improved Synthesis of 4-Bromo-2,2'-Bipyridine: A Start Material for Low-Molecular-Weight Model Compounds. *Designed Monomers and Polymers* **2001**, *4*(2), 169–175.

(23) Wenkert, D.; Woodward R.B. Studies of 2,2'-Bypyridyl N,N'-Dioxides. *J. Org. Chem.* **1983,** *48*, 0022-3263.

(24) Bair, J. S.; Harrison, R. G. Synthesis and Optical Properties of Bifunctional Thiophene Molecules Coordinated to Ruthenium. *J. Org. Chem.* **2007**, *72* (18), 6653–6661.

(25) Takeda, H.; Koike, K.; Inoue, H.; Ishitani, O. Development of an Efficient Photocatalytic System for CO2 Reduction Using Rhenium(I) Complexes Based on Mechanistic Studies. *J. Am. Chem. Soc.***2008**, *130* (6), 2023–2031.

(26) Genoni, A.; Chirdon, D. N.; Boniolo, M.; Sartorel, A.; Bernhard, S.; Bonchio, M. Tuning Iridium Photocatalysts and Light Irradiation for Enhanced CO2 Reduction. *ACS Catal.* **2017**, *7* (1), 154–160.

Experimental synthesis

All the succeeding synthetic procedures were prepared according to the relative literature procedures. [7,21-26]

2,2'-Bipyridyl *N*-Oxide (1b): A solution of (7 g, 44.82 mmol) 2,2-bipyridine in 25 mL of chloroform was prepared in a 100 mL two neck round bottom flask and stirred at 0°C in air for 35 mins. Another solution of (9.156 g, 53.05 mmol) *m*-chloroperbenzoic acid in 87 mL of chloroform was prepared and added to the flask dropwise using a dropping funnel over a period of 80 mins. The mixture was allowed to stir at room temperature for 14 hours. The resulting solution was washed three time with 5% Na_2CO_3 solution and extracted three times with chloroform. The chloroform layer was evaporated to dryness which resulted in a brown oily product. The remaining unreacted reactants which was in the residual oil was treated with boiling hexane. The hexane layer was carefully removed using the process of decantation and rotary evaporation. The greyish brown product was left to dry under the house vacuum overnight which obtained a percentage yield of 70%.

4-Nitro-2,2'-bipyridyl *N*-Oxide(1c): (1 g, 5.81 mmol of 2,2'-Bipyridyl *N*-Oxide) was dissolved in 12.5 mL of H_2SO_4 and the mixture was stirred and heated in air at 100°C. 3 mL concentrated HNO_3 was dripped over several minutes and the reaction was heated under reflux for 3 days at 70 °C. After cooling the solution, it was poured in ice and then cooled in the ice bath. The addition of NaOH pallets in the solution to neutralize at pH 9 is highly exothermic so extreme precaution was taken. The resulting precipitate was filtered through the glass frit, washed with cold distilled water and left to dry on air for a day which obtained a percentage yield of 35%.

4-Bromo-2,2'-bipyridine (1d): (1.54 g, 7.06 mmol) of 4-Nitro-2,2'-bipyridyl *N*-Oxide was dissolved in 25 mL of glacial acetic acid. After the solution was degassed for 35 mins, 5 mL acetyl bromide was added to the mixture with constant stirring under nitrogen which yielded a yellow precipitate. After 20 mins, 5 mL of phosphorous tribromide was added to the resulting solution which caused the precipitate to re-dissolve. The solution was heated under reflux for 2.5 hours at 118 ^{o}C. After cooling to room temperature, the solution was decanted, and the remaining sticky product was dissolved in ice cold water. The acidic solution was neutralized to pH 9 using NaOH pallet which was then extracted with DCM three times. The DCM layer was then evaporated to dryness to obtain the product with a yield of 79%.

Mononuclear catalyst (1f)

4-(anthracen-9-yl)-2,2'-bipyridine (L1) (1e): (1.148 mL of 1.5 M) K_2CO_3 and 1.88 mL of ethanol were degassed together in a round bottom flask for 30 mins. (0.15 g, 0.675 mmol) 9-Anthraceneboronic acid and (0.2 g, 0.85 mmol) 4-bromo-2,2'-bipyridine along with 5 mL of anhydrous toluene was degassed separately in a two neck round bottom flask for 15 mins. The degassed solvents were added into the main mixture and the reaction mixture was heated for a day at 100^{0}C. After the reaction was completed and cooled at room temperature, 1.94 mL of saturated aqueous NH_4Cl and 1.94 mL of H_2O were added which was then extracted several times with DCM and evaporated to dryness to get yellow powder. A silica gel chromatography column was run with 5:1 Hx:EtOAc for purification which obtained a yield of 62%. ^{1}H NMR (500 MHz, DMSO-d_6): δ 9.24 (d, J = 5.55 Hz, 1H), 9.10 (d, J = 5.95 Hz, 1H), 9.01 (s, 1H), 8.87 (s, 1H), 8.84 (d, J = 8.1 Hz, 1H), 8.27 (m, J = 8.35, 9.2 Hz, 4H), 7.88 (d, J = 5.5 Hz, 1H), 7.78 (m, J = 7.0, 6.6

Hz, 1H), 7.70 (d, J = 9.0 Hz, 1H), 7.58 (ddd, J = 7.2, 8.0, 6.35, 7.5, 6.25, 8.3, 7.05, 7.4 Hz, 6H), 7.44 (d, J = 7.8 Hz, 1H).

Re [L1] $(CO)_3Cl$ (1f): (50 mg, 0.15 mmol) 4-(anthracen-9-yl)-2,2'-bipyridine was stirred in 5 ml of toluene and degassed for 15 mins. After 15 mins, (54.25 mg 0.15 mmol) $Re(CO)_5Cl$ was added in the mixture under the positive pressure of N_2 which was then refluxed at 115 ^oC overnight. The precipitated metal ligand complex was then filtered and washed with hexane which obtained a yield of 78%. ^1H NMR (500 MHz, DMSO-d_6): δ 8.96 (d, J = 4.25 Hz, 1H), 8.79 (s, 1H), 8.61 (d, J = 2.9 Hz, 1H), 8.57 (d, J = 7.6 Hz, 1H), 8.41 (s, 1H), 8.21 (d, J = 8.25 Hz, 2H), 8.02 (t, J = 7.3, 8.35 Hz, 1H), 7.57 (m, J = 6.1, 8.3 Hz, 5H), 7.49 (d, J = 7.0, 6.7 Hz, 4H). ^{13}C NMR (126 MHz, DMSO-d_6): δ 198.32, 190.59, 156.38, 155.83, 153.30, 151.10, 140.74, 131.84, 131.15, 130.60, 129.25, 128.89, 128.44, 127.59, 127.47, 127.22, 126.22, 126.06, 125.22.

1,8-bis(neopentylglycolatoboryl)anthracene (2b): A solution of (0.75 g, 4.05 mmol) 1,8-dichloroanthracene, (2.3 g, 10 mmol) bis(neopentyl-glycolato)diborane, (0.083 g, 0.08 mmol) of $Pd_2(dba)_3$, (0.1525 g, 0.32 mmol) of 2-Dicyclohexylphosphino-2',4',6'-triisopropylbiphenyl and (4.15 g, 50.5) mmol of NaOAc in 35 mL of anhydrous 1,4-dioxane was heated at 90 ^oC under N_2 for two days. The product was rotavaped to dryness. Toluene was added to the flask and the insoluble precipitate was filtered off. After the volume of the toluene was reduced, 6 mL of hexane was layered on the toluene and allowed to stand for 1 day in the fridge to generate crystals. The crystals were then collected in the frit using vacuum filtration which obtained a yield of 74%.

Dinuclear complex

1,8-di([2,3'-bipyridin]-4yl)anthracene (L2) (2c) : 0.776 mL of 1.5 M K_2CO_3 and 1.5 mL of ethanol were degassed together in a round bottom flask for 30 mins. (0.078 g, 0.194 mmol) 1,8-

bis(neopentylglycolatoboryl)anthracene and (0.11 g, 0.467 mmol) 4-bromo-2,2'-bipyridine along with 5 mL of anhydrous toluene was degassed separately in a two neck round bottom flask for 15 mins. The degassed solvents were added into the main mixture and the reaction mixture was allowed to reflux for a day at 100 ^{o}C. After the reaction was completed and cooled at room temperature, 1.94 mL of saturated aqueous NH_4Cl and 1.94 mL of H_2O were added which was then extracted several times with DCM and evaporated to dryness to get yellow powder. Two different silica gel chromatography were run to obtain two different pure enantiomers. The first column was run with 5:1 Hx:EtOAc whereas the second deactivated column was run with 2.5:1-Hx:EtOAc which obtained a yield of 46%. ^{1}H NMR (500 MHz, DMSO-d_6): δ 9.12 (s, 1H), 9.02 (q, J = 13.05, 6.1, 7.8 Hz, 4H), 8.91 (d, J = 8.25 Hz, 1H), 8.86 (m, J = 5.05, 5.3 Hz, 1H), 8.76 (d, J = 5.4 Hz, 1H), 8.66 (d, J = 13.85 Hz, 1H), 8.39 (dd, J = 8.75, 7.9, 8.25,6.6 Hz, 2H), 8.25 (m, J = 7.65, 6.75 Hz, 1H), 8.11 (s, 2H), 7.80 (dt, J = 4.0, 4.65, 3.3, 6.4, 6.65 Hz, 4H), 7.73 (m, J = 6.9, 5.9 Hz, 1H).

Re_2 [L2] $(CO)_6Cl_2$ (2d): (50 mg, 0.103 mmol) 1,8-di([2,3'-bipyridin]-4yl)anthracene was stirred in 5 mL of toluene and degassed for 15 mins. After 15 mins, (24.33mg, 0.206 mmol) $Re(CO)_5Cl$ was added in the mixture under the positive pressure of N_2 which was then refluxed at 115 ^{o}C overnight. The precipitated metal ligand complex was then filtered and washed with hexane which obtained a yield of 61%. Here, we were unable to separate two distinct isomers, therefore, all the characterization and experimental studies were performed using this isomeric mixture. ^{1}H NMR (500 MHz, Acetone-d_6): δ 8.85 (s, 1H), 8.76 (s, 1H), 8.65 (m, J = 9.35, 4.4, 4H), 8.94 (d, J = 7.9 Hz, 2H), 8.33(d, J = 4.8 Hz, 2H), 8.28(d, J = 8.55 Hz, 2H), 7.96 (t, J = 7.55, 7.9 Hz, 2H), 7.71(m, J = 6.85, 8.4 Hz, 2H), 7.65 (d, J = 7.6 Hz, 3H) , 7.42 (m, J = 4.6, 7.7 Hz, 2H).

^{1}H NMR data

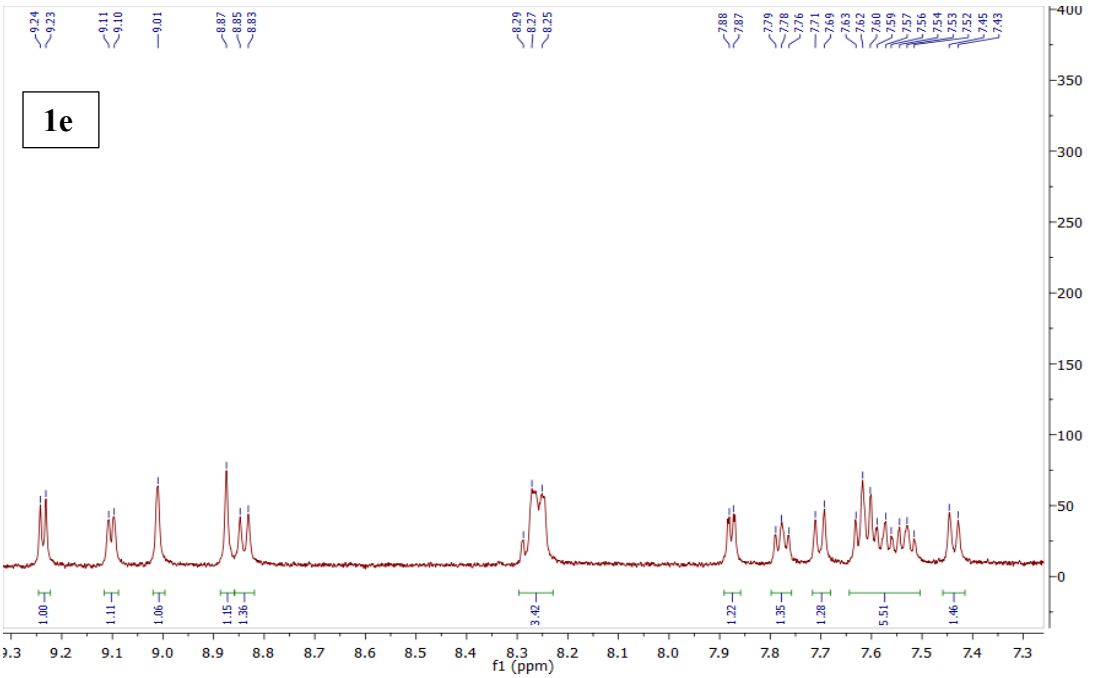
1e
9.24
9.23
9.11
9.10
9.01
8.87
8.85
8.83
8.29
8.27
8.25
7.88
7.87
7.79
7.78
7.76
7.71
7.69
7.63
7.62
7.60
7.59
7.57
7.56
7.54
7.53
7.52
7.45
7.43
1.00
1.11
1.06
1.15
1.36
3.42
1.22
1.35
1.28
5.51
1.46
f1 (ppm)

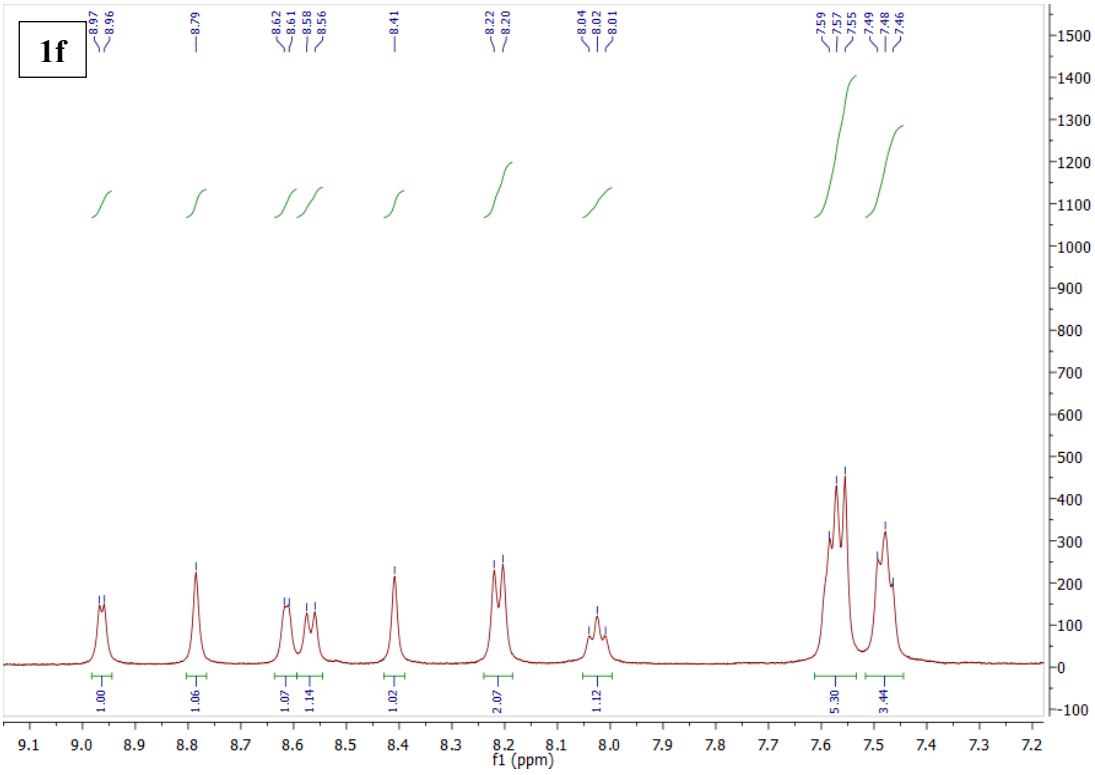
1f
8.97
8.96
8.79
8.62
8.61
8.58
8.56
8.41
8.22
8.20
8.04
8.02
8.01
7.59
7.57
7.55
7.49
7.48
7.46
1.00
1.06
1.07
1.14
1.02
2.07
1.12
5.30
3.44
f1 (ppm)

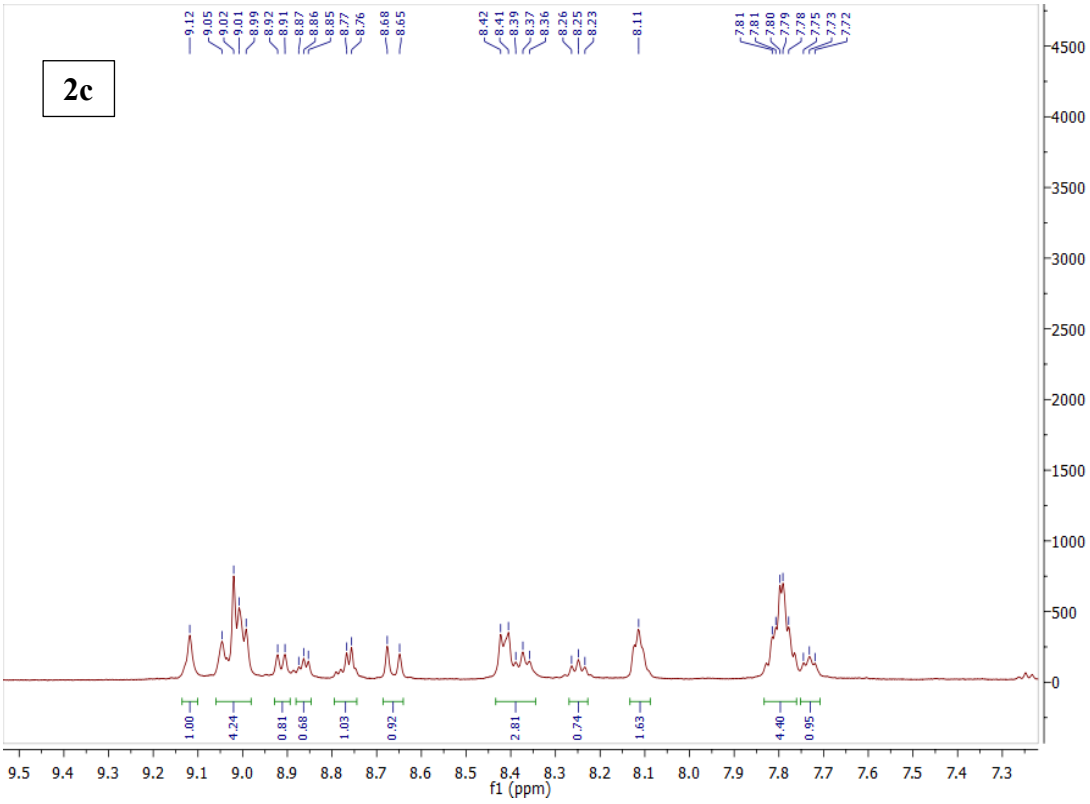
2c
9.12
9.05
9.02
9.01
8.99
8.92
8.91
8.87
8.86
8.85
8.77
8.76
8.68
8.65
8.42
8.41
8.39
8.37
8.36
8.26
8.25
8.23
8.11
7.81
7.81
7.80
7.79
7.78
7.75
7.73
7.72
1.00
4.24
0.81
0.68
1.03
0.92
2.81
0.74
1.63
4.40
0.95
f1 (ppm)

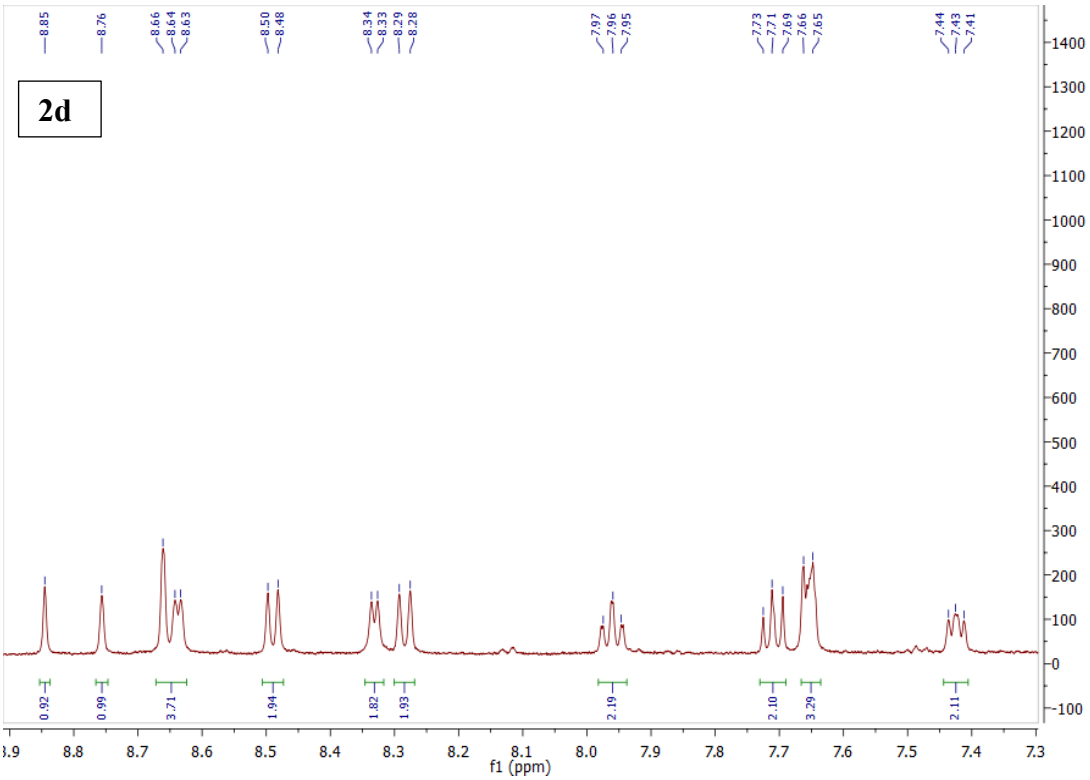
2d
8.85
8.76
8.66
8.64
8.63
8.50
8.48
8.34
8.33
8.29
8.28
7.97
7.96
7.95
7.73
7.71
7.69
7.66
7.65
7.44
7.43
7.41
0.92
0.99
3.71
1.94
1.82
1.93
2.19
2.10
3.29
2.11
f1 (ppm)

^{13}C NMR data

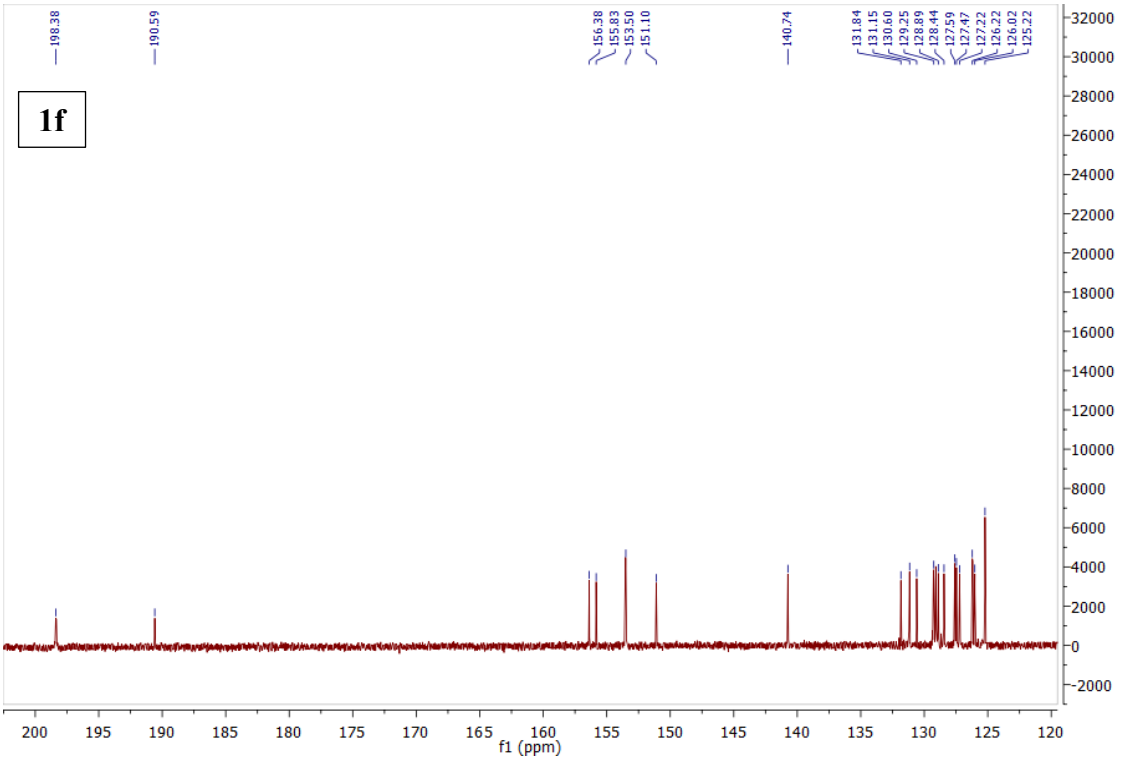
198.38
190.59
156.38
155.83
153.50
151.10
140.74
131.84
131.15
130.60
129.25
128.89
128.44
127.59
127.47
127.22
126.22
126.02
125.22
1f
f1 (ppm)